11-30-2008

Macroalgae and eelgrass mapping in Great Bay Estuary using AISA hyperspectral imagery

Shachak Pe'eri
Center for Coastal Ocean Mapping

J. Ru Morrison
Coastal Observing Center

Frederick T. Short
Jackson Estuary Laboratory University of New Hampshire, fred.short@unh.edu

Arthur C. Mathieson
Jackson Estuary Laboratory University of New Hampshire, Arthur.Mathieson@unh.edu

Anna Brook
The Department of Geography and Human Environment Tel Aviv University

See next page for additional authors

Authors
Shachak Pe'eri, J. Ru Morrison, Frederick T. Short, Arthur C. Mathieson, Anna Brook, and Philip Trowbridge

Macroalgae and eelgrass mapping in Great Bay Estuary using AISA hyperspectral imagery

A Final Report to

The New Hampshire Estuaries Project

Submitted by

Shachak Pe'eri[1]
J. Ru Morrison[2]
Fred Short[3]
Arthur Mathieson[3]
Anna Brook[4]
Philip Trowbridge[5]
[1]Center for Coastal Ocean Mapping
[2]Coastal Observing Center
[3]Jackson Estuary Laboratory
University of New Hampshire
Durham, NH
[4]The Department of Geography and Human Environment
Tel Aviv University
[5]New Hampshire Estuaries Project

November, 30 2008

This project was funded in part by a grant from the New Hampshire Estuaries Project as authorized by the U.S. Environmental Protection Agency's National Estuary Program.

Table of Contents

1 Abstract (400 words or less)

Increase in nitrogen concentration and declining eelgrass beds in Great Bay Estuary have been observed in the last decades. These two parameters are clear indicators of the impending problems for NH's estuaries. The NH Department of Environmental Services (DES) in collaboration with the New Hampshire Estuaries Project (NHEP) adopted the assumption that eelgrass survival can be used as the water quality target for nutrient criteria development for NH's estuaries. One of the hypotheses put forward regarding eelgrass decline is that a possible eutrophication response to nutrient increases in the Great Bay Estuary has been the proliferation of nuisance macroalgae, which has reduced eelgrass area in Great Bay Estuary. To test this hypothesis, mapping of eelgrass and nuisance macroalgae beds using hyperspectral imagery was suggested.

A hyperspectral imagery was conducted by SpecTIR in August 2007 using an AISA Eagle sensor. The collected dataset was used to map eelgrass and nuisance macroalgae throughout the Great Bay Estuary. This report outlines the configured procedure for mapping the macroalgae and eelgrass beds using hyperspectral imagery. No ground truth measurements of eelgrass or macroalgae were collected as part of this project, although eelgrass ground truth data was collected as part of a separate project. Guidance from eelgrass and macroalgae experts was used for identifying training sets and evaluating the classification results. The results produced a comprehensive eelgrass and macroalgae map of the estuary. Three recommendations are suggested following the experience gained in this study: conducting ground truth measurements at the time of the HS survey, acquiring the current DEM model of Great Bay Estuary, and examining additional HS datasets with expert eelgrass and macroalgae guidance. These three issues can improve the classification results and allow more advanced applications, such as identification of macroalgae types.

2 Executive Summary

Measurements over the last few decades demonstrated an increased nitrogen concentration in Great Bay (59% in the past 25 years) and a loss in percent cover of historic eelgrass beds (29% in the past 60 years). Increasing nitrogen concentrations and declining eelgrass beds in Great Bay are clear indicators of impending problems for NH's estuaries. One of the NH Department of Environmental Services (DES) responsibilities is nutrient criteria development for protecting NH's estuaries. The DES, in collaboration with the New Hampshire Estuaries Project (NHEP), adopted the assumption that eelgrass survival can be used as a water quality target for nutrient criteria development for NH's estuaries. Eelgrass takes up a large portion of nitrogen from the water column in Great Bay, but as nitrogen levels have risen and exceeded the capacity of eelgrass to absorb; researchers have observed a proliferation of green and red nuisance macroalgae and a loss of eelgrass.

A study was suggested by the DES to test the hypothesis that one of the eutrophication responses to nutrient increases in the Great Bay Estuary has been a proliferation of abundance of macroalgae, which has reduced the amount of eelgrass the Great Bay Esuary. Hyperspectral imagery collected in August and October 2007 was used to map eelgrass and nuisance macroalgae throughout the estuary. The distribution of nuisance macroalgae will be compared to areas where historic eelgrass beds have been lost to determine whether nuisance macroalgae correlates with eelgrass loss in the Great Bay Estuary. The research outputs will contribute to the development of numeric nutrient criteria for NH's estuaries. The research will benefit other states in New England because eutrophication responses in Great Bay Estuary can be used as a model for other, macrotidal estuaries.

This report outlines a procedure for mapping the macroalgae and eelgrass beds using hyperspectral imagery. The procedure was configured based on the available hyperspectral data on the study site (Great Bay Estuary). No ground truth measurements of eelgrass or macroalgae were collected as part of this survey. This present study required guidance from eelgrass and macroalgae experts in identifying training sets and evaluating the classification results. The goals of the study were to configure a procedure for identifying eelgrass and macroalgae based on AISA hyperspectral remote sensing imagery; map eelgrass and macroalgae beds using data collected from 2008 NHDES hyperspectral survey; and provide a recommendation for planning future hyperspectral surveys for eelgrass mapping based on the study experience. The eelgrass and macroalgae mapping procedure included four main tasks:

- End-member collection- A spectrum representing a spectrally "pure" feature (e.g, vegetation, soil, etc.) is defined as a spectral end-member. Candidate locations were identified in the hyperspectral imagery and end-members were created of the macroalgae and eelgrass areas and of bottoms without macroalgae (pure background).

- Endmember analysis- The collected end-members were analyzed according to the feature type. Distinct features along the spectra were used to discriminate between the different end-members.

- Classification- Following the characteristics of the different end-members a classification technique approach (decision rules) was chosen and applied to the data. The classification algorithms and algorithm thresholds were modified following several iterations with eelgrass and macroalgea experts. The resulting product is a thematic map that represents spatial distribution of the eelgrass and macroalgae beds.

- Data export- The classification results were exported to a vector format that is compliant with the GIS environment (shapfile polygons).

The resulting product of the study was the development of a mapping procedure for eelgrass and macroalgae. This procedure included four main processing steps (not including pre-processing): 1) water body separation from land, 2) mapping the vegetation in the water body, 3) masking wetland vegetation, and 4) mapping the eelgrass and macroalgae beds. The resulting classes (eelgrass and macroalgea) were merged into a single file and georefenced to WGS-84 datum with a UTM projection (Zone 19N). The georeferenced class files were exported to an ArcMap-polygon shapefile. The shapefiles were subset into the NHDES estuary assessment zones and all files were also georeferenced to the New Hampshire State Plane NAD 1983 (FIPS 2800). Given the quality of the data and time constraints associated with funding available for the work, only the overflight on August 29, 2007 was analyzed.

A comprehensive eelgrass and macroalgae map of the Estuary was produced. The classification process was not automatic and required interaction with the operator. Important wavelength regions for the procedure were identified (0.574 µm to 0.630 µm and 0.670 µm to 0.726 m). Three recommendations are suggested following the experience gained in this study:

1. Collection of ground truth (reflectance spectra) at the time of the hyperspectral survey would allow QA of the dataset, applying water depth correction to the dataset, and constructing decision rules for classification.

2. An updated high resolution (2.5 m) elevation model that also covers the shallow areas would allow correcting the HS dataset attenuation at different water depths.

3. Additional hyperspectral datasets over the same study area and also other sites that contain eelgrass and macroalgae would provide more feedback on the procedure and allow it to be more robust.

4. Ground truth assessments simultaneous with the HS imagery and substantial expert eelgrass and macroalgae input are needed to increase the level of confidence in the HS image analysis.

The results of the HS study including maps of eelgrass and macroalgae can now be compared to the historic eelgrass maps and to the 2007 ground-truthed eelgrass maps, in order to evaluate the success of the image analysis and determine the areas of former eelgrass that are now macroalgae.

3 List of Tables

4 List of Figures

5 Introduction (Great Bay Estuary without Portsmouth Harbor)

5.1 Importance of eelgrass mapping

Nitrogen concentration in Great Bay Estuary (GBE) has increased by 59% in the past 25 years (NHEP, 2006). Since the 1940s, 29% of the historic eelgrass cover has been lost. Nitrogen loading rates in GBE (182 kg/ha/yr) are higher than estuaries for which dramatic eelgrass loss has occurred (>60 kg/ha/yr) (Hauxwell et al., 2003). Increasing nitrogen concentrations (Figure 5.1) and declining eelgrass beds in GBE (Figure 2) are clear indicators of impending problems for NH's estuaries (Short et al. 1986, Short 1992, NHEP, 2006). The NH Department of Environmental Services (DES) in collaboration with the New Hampshire Estuaries Project (NHEP) began developing nutrient criteria for NH's estuaries with the formation of a workgroup in 2005. This workgroup adopted eelgrass survival as the water quality target for nutrient criteria development for NH's estuaries. The results of the study will aid in the development of numeric nutrient criteria. A research goal of NHEP is to investigate if the proliferation of nuisance macroalgae is a result of eutrophication response (increase in nutrients) in the GBE. Eelgrass takes up a large portion of nitrogen from the water column, but as nitrogen levels have risen, researchers have observed a proliferation of green and red nuisance macroalgae. Macroalgae can eliminate eelgrass when it forms dense mats on the sediment (Short and Burdick 1996) and can prevent the reestablishment of eelgrass in potential habitat areas.

This report presents the results of mapping eelgrass and macroalgae beds in GBE. The surveying technique used to map the eelgrass and macroalgae beds was airborne hyperspectral remote sensing. Hyperspectral Imaging is part of a class of remote sensing techniques commonly referred to as spectral imaging or spectral analysis. Hyperspectral sensors collect information as a set of 'images'. Each image represents a range of the electromagnetic spectrum and is also known as a spectral band. These 'images' are then combined and form a three dimensional hyperspectral cube for processing and analysis. The ability of hyperspectral imaging to identify various minerals and other chemical compositions by spectral analysis makes it a useful tool for this study.

In 2007, the NHEP received a 104(b)(3) grant from the U.S. Environmental Protection Agency (EPA) to collect water quality information including that from hyperspectral imagery data of the GBE (EPA Grant Award X7-97167001). The NHEP collected hyperspectral imagery and water quality data from the GBE in 2007 (August and October 2007) (Figure 3). Data was collected under an approved QAPP. This report summarizes the analysis of the hyperspectral imagery data conducted by researchers from NHEP and the University of New Hampshire. This is the first time that a quantified spatial macroalgae mapping has been conducted throughout the estuary using a standard, synoptic method. Results of this research will contribute to the development of numeric nutrient criteria for NH's estuaries. In addition to New Hampshire, the research will benefit other states in New England because eutrophication responses in GBE can be used as a model for other northern, macrotidal estuaries.

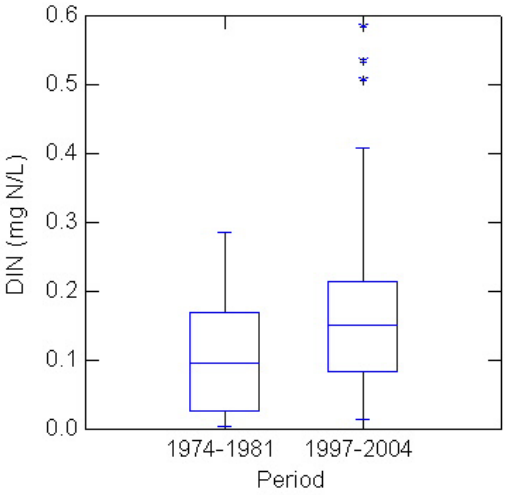

Figure 5.1 Dissolved inorganic nitrogen concentrations in Great Bay (NHEP, 2006)

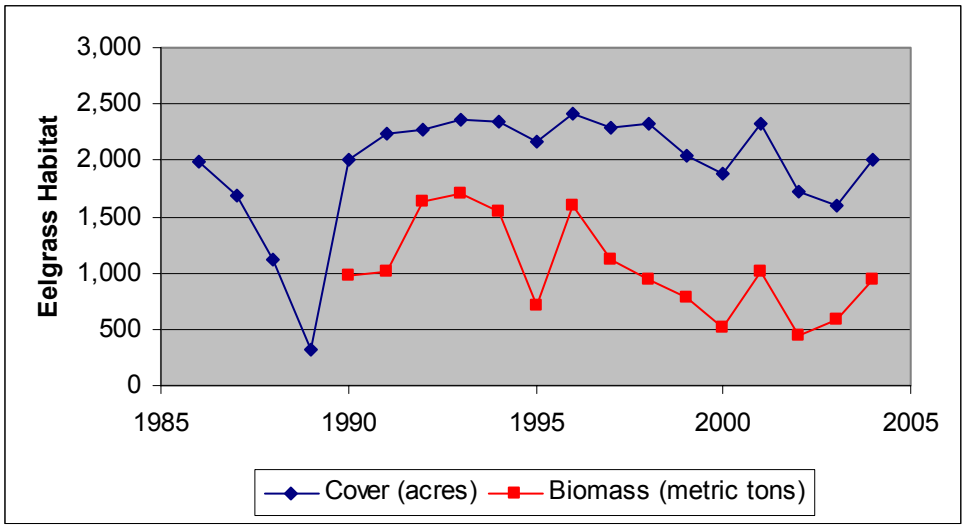

Figure 5.2 Eelgrass cover and biomass in Great Bay (NHEP, 2006)

5.2 Hyperspectral Remote Sensing in Shallow waters

Hyperspectral (HS) remote sensing theoretically contains continuous spectral observations and practically has observations every 5 to 10 nm typical of AVIRIS, AISA, PHILLS, and CASI airborne instruments. These sensors typically have tens to hundreds of spectral channels in the ultraviolet (UV), visible, near infrared (NIR), and the short wave infrared (SWIR) wavelengths. Successfully used for many years with terrestrial applications, this technology has only recently been applied to applications in aquatic systems including those of coastal oceans (Lee and Carder 2005). Inversion of reflectance signatures in these environments is often complicated as the water column and bottom both contribute to the water leaving radiance with their relative contributions

being modulated by water depth (e.g., Lyzenga 1981; Maritorena et al. 1994). A number of approaches have been used for such inversions including; reflectance ratio algorithms (Dierssen et al. 2003), neural networks (Sandage and Holyer 1998), spectral optimization (Lee et al. 2001; Lee et al. 1998; Lee et al. 1999), and spectrum matching and look-up table (LUT, Lesser and Mobley 2007; Louchard et al. 2003; Mobley et al. 2005). Most of these studies have been performed in relatively clear waters surrounding coral reef environments.

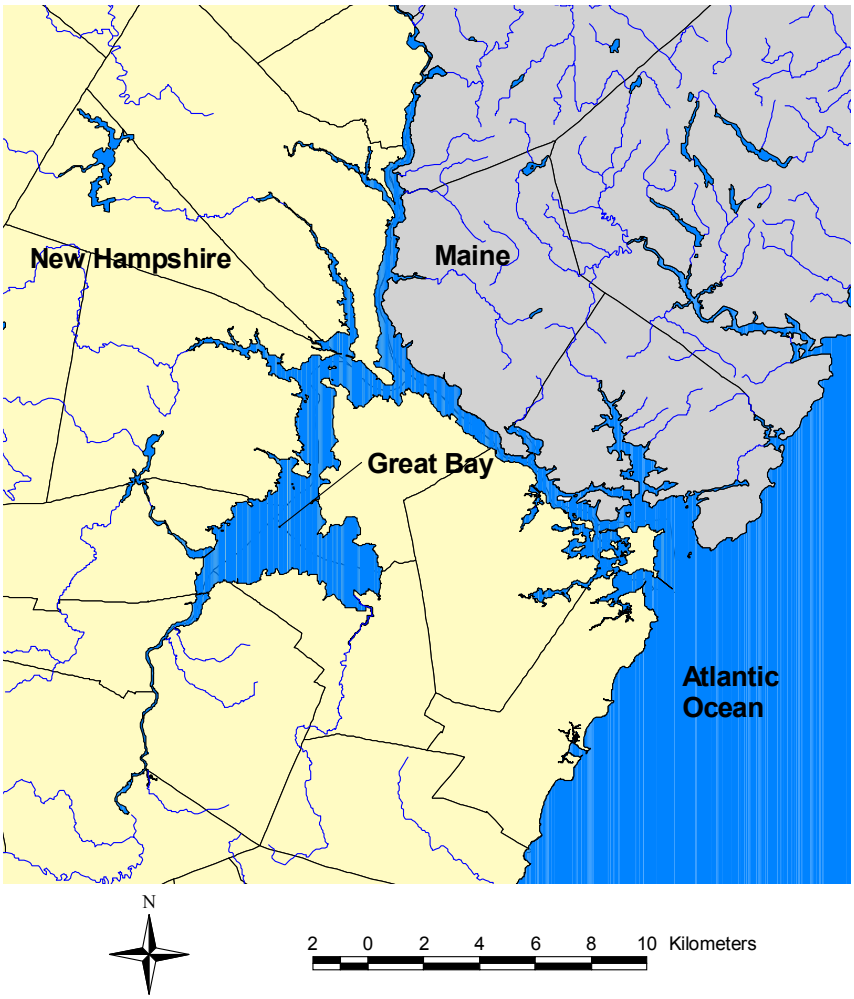

Figure 5.3 The Great Bay Estuary

Spectral optimization and the LUT protocols both need information on the range of Inherent Optical Properties (IOPs) of the water column and the bottom reflectance or albedo. However, they differ in how these are used to model and invert remotely measured reflectance. Of the IOPs the absorption and backscattering coefficients (a and bb, respectively) are most important in remote sensing (Gordon et al. 1988). IOPs are determined in part by water but also by other optically important constituents and can be modeled as proportional to constituent concentrations (Mobley 1994). Optically

important in-water constituents include phytoplankton, non-algal particles (both organic and inorganic), and colored dissolved organic matter (CDOM). Bottom reflectance, ρ, depends on the relative contributions of differing substrate types (e.g. sand, seagrass, macrophytic algae, and coral). The LUT approach uses ranges of constituents, bottom reflectance for differing substrates (and mixtures thereof), and depths with a radiative transfer model such as Hydrolight (Mobley 1994) to predict surface reflectances a priori for a range of conditions. For example, 28 sets of IOPs, 84 depths, and 118 bottom reflectance spectra yielded 275,000 spectra in an LUT (Lesser and Mobley 2007). By matching observed reflectance spectra to the nearest one in the LUT the water column and benthic properties as well as bathymetry are retrieved. In contrast, spectral optimization techniques use a semi-analytical iterative inversion approach to vary water depth, water column optical constituents, and potentially bottom type to minimize differences between observed and predicted spectra. Lee et al. (2001) only used two bottom types, sand and seagrass, with the bottom reflectance selected before minimization using the remotely sensed reflectance spectra. Goodman and Ustin (2008) used a three-step process to further classify benthic composition. First, a generic bottom reflectance and spectral optimization to invert for water properties and bathymetry; second, these products were used to predict the actual bottom reflectance; and third a linear spectral unmixing model was used for benthic classification.

Both LUT and spectral optimization (with unmixing) have demonstrated capacity to retrieve important water column and benthic properties. For example, for each pixel a percent contribution to the bottom reflectance of different substrate and biological cover is possible allowing abundance estimates. However, knowledge of water column optical properties, bottom reflectance and / or bathymetry before the reflectance spectra inversion has the potential to decrease processing time (Mobley et al. 2005) and reduce uncertainties in the retrieved products. This can be expressed in a simple radiative transfer model for optically shallow waters of the general form (Philpot, 1989; Mobley, 1994):

$$L_d = L_b \exp(-Kz) + L_w$$

where L_d is the radiance observed at the remote detector, K is the effective attenuation coefficient of the water, z is depth of the water column, L_b = a radiance term which is sensitive to bottom reflectance, and L_w = remotely observed radiance over optically deep water ($gz \rightarrow \infty$).

5.3 Spectral responses of eelgrass and macroalgae

The potential use of spectral instruments for mapping eelgrass and macroalgae has been recognized by studies conducted in the past (Haxo and Blinks, 1950; Gitelson, 1992; Rundquist et al., 1996; Zimmerman, 2003; Alberotanza et al., 2006; Thorhaug et al., 2007). Most of the work employed data between 400 nm and 800 nm. Unfortunately, only limited work was done for defining a procedure to map eelgrass and macroalgae using airborne or satellite imagery (Alberotanza et al., 2006).

Knowledge of light scattering by plant canopies is crucial for remote sensing quantification of vegetation abundance and distribution, as well as for the development of inversion techniques to infer plant chemical composition, which is important for ecosystem-scale estimates of plant growth and biogeochemical flux (Jacquemoud et al. 1996; LaCapra et al.1996; Broge and Leblanc 2000).

Pigments, such as chlorophylls, carotenoids, and phycobilins are considered as the vegetation substances responsible for the absorption of light. Studies on submerged vegetation observed similar spectral characteristics. These characteristics as a function of wavelength are commonly summarized as follows:

- **0.400 to 0.500 µm** - Low reflectivity due to the absorption of blue light (maximum absorption at about 440 nm).
- **0.550 to 0.570 µm** - Maximum green reflectivity.
- **0.660 to 0.690 µm** - Low reflectivity due to red light absorption (maximum absorption between 670 and 680 nm).
- **0.755 to 0.765 µm** - Low reflectivity in the near infrared during pigmentation phase. An increasing of reflectivity occurs during blooming periods and in emerged vegetation conditions.

Chlorophyll-a is also a predominant pigment in benthic macroalgae and similar absorption peaks are noticed at wavelength of 440, 675, 695 nm. Other major pigments are phycoerythrin found in red macroalgae (absorption peak at 565 nm), phycocyanin found in red and blue-green algae (absorption peak at 620 nm), fucoxanthin (absorption peak at 470 nm) (Wezermak et al., 1976). Examples of spectra of eelgrass and macroalgae are presented in Figures 5.4 and 5.5.

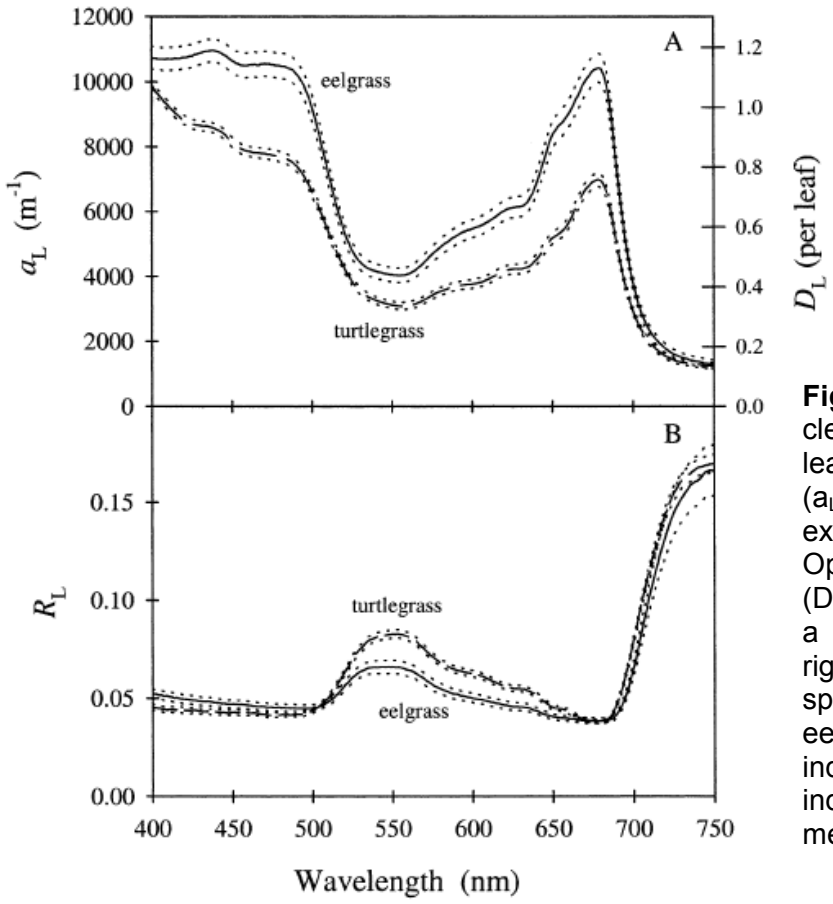

Figure 5.4 A) Absorption spectra of clean turtlegrass and eelgrass leaves. Leaf absorption coefficients (a_L, left vertical axis) were expressed m^{-1} of leaf thickness. Optical densities, or absorbances (D_L), normalized to the thickness of a single leaf, were scaled on the right vertical axis. (B) Reflectance spectra of clean turtlegrass and eelgrass leaves. Solid lines indicate mean spectra; dotted lines indicate standard errors of the means (from Zimmerman, 2003).

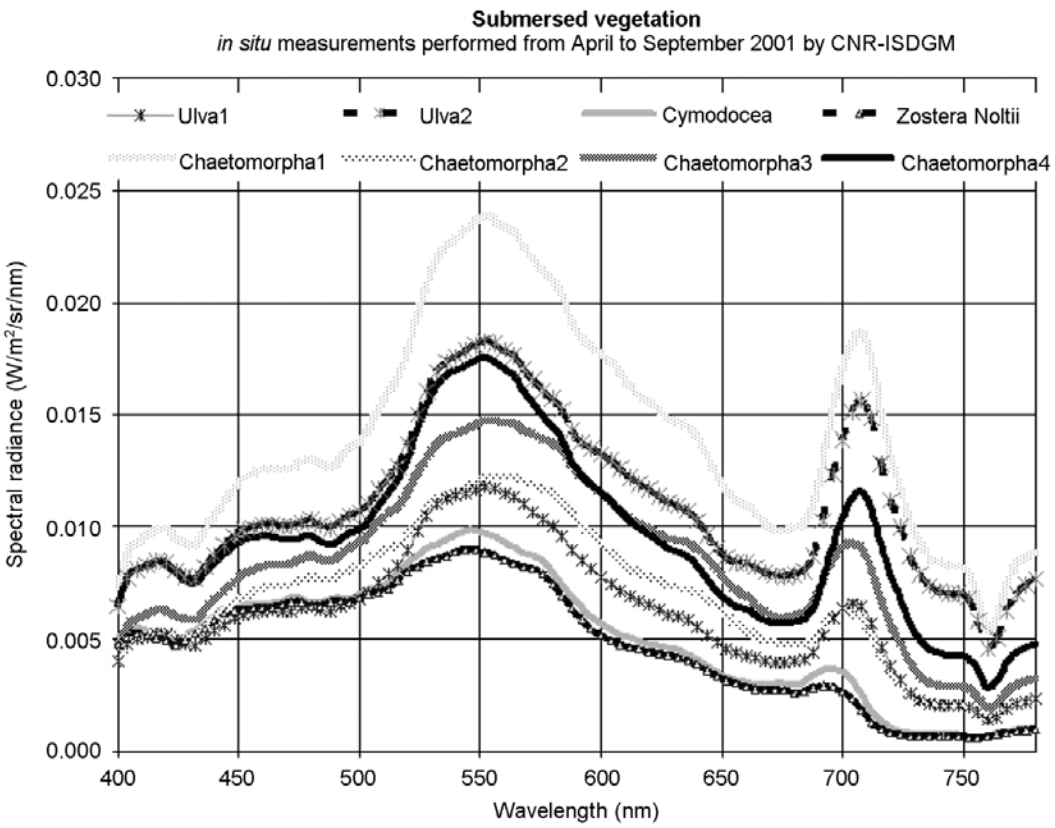

Figure 5.5 Radiance spectra of submersed vegetation and macroalgae (Alberotanza et al., 2006).

6 Project Goals and Objectives

The project goals were:

a) Configure a procedure for identifying eelgrass and macroalgae based on AISA hyperspectral remote sensing imagery;

b) Map eelgrass and macroalgae beds using data collected from 2008 NHDES hyperspectral survey; and

c) Provide a recommendation for planning future hyperspectral surveys for eelgrass mapping based on the study experience.

7 Methods

7.1. Introduction

The hyperspectral imagery collected information for the Great Bay estuarine system of NH and Maine. This area encompassed the Great Bay, Little Bay, Piscataqua River and some or all of the tidal portions of the Winnicut, Squamscott, Lamprey, Oyster, Bellamy, Cocheco and Salmon Falls Rivers. Approximately 40 square kilometers of estuarine waters were part of the study area. The initial plans were to collect imagery during two differing flow regimes for the estuarine system during low-flow summer and higher-flow fall conditions. The goal was also to collect data at either high or low tide when temporal consistency would be maximal.

The over-flights were conducted by SpecTIR (www.SpecTIR.com). SpecTIR proposed an airborne data collection with the VNIR sensor with a spatial resolution of 2.5 meters for the area of interest, and a nominal spectral resolution of 10 nm or 64 spectral channels from approximately 430 nm to 1000 nm (Table 7.1). Navigation was performed with high speed airborne DGPS integrated with a laser ring gyro and deliverables were calibrated radiance and geographic lookup tables with navigation. Overlap of 30% was planned between two adjacent lines. SpecTIR also recommended that over-flights should coincide with solar zenith angles less than 60º to minimize sun-glint contamination and have minimal cloud cover. The flight lines are presented in Figure 7.1 and flight log details are provided in Appendix 11.1.

Table 7.1 Acquisition parameters for the hyperspectral data collection

Sensor System:	ProSpecTIR-V (AISA eagle)
Spectral Range:	400 nm - 1000 nm
Spectral Resolution:	10 nm
Number of Bands:	64
Ground Spatial Distance (GSD):	2.5 m

The next sub-sections will discuss the steps required for processing the collected hyperspectral dataset. An image-processing software (ENVI) was used for processing and analyzing the geospatial imagery dataset. The produced class files (eelgrass and macroalgae) were exported into ArcMap shapefile format. Unfortunately, no spectral ground truth measurements of eelgrass or macroalgae were taken as part of this study. Decision rules for processing were based on spectra collection from pixels identified of different features in the study site.

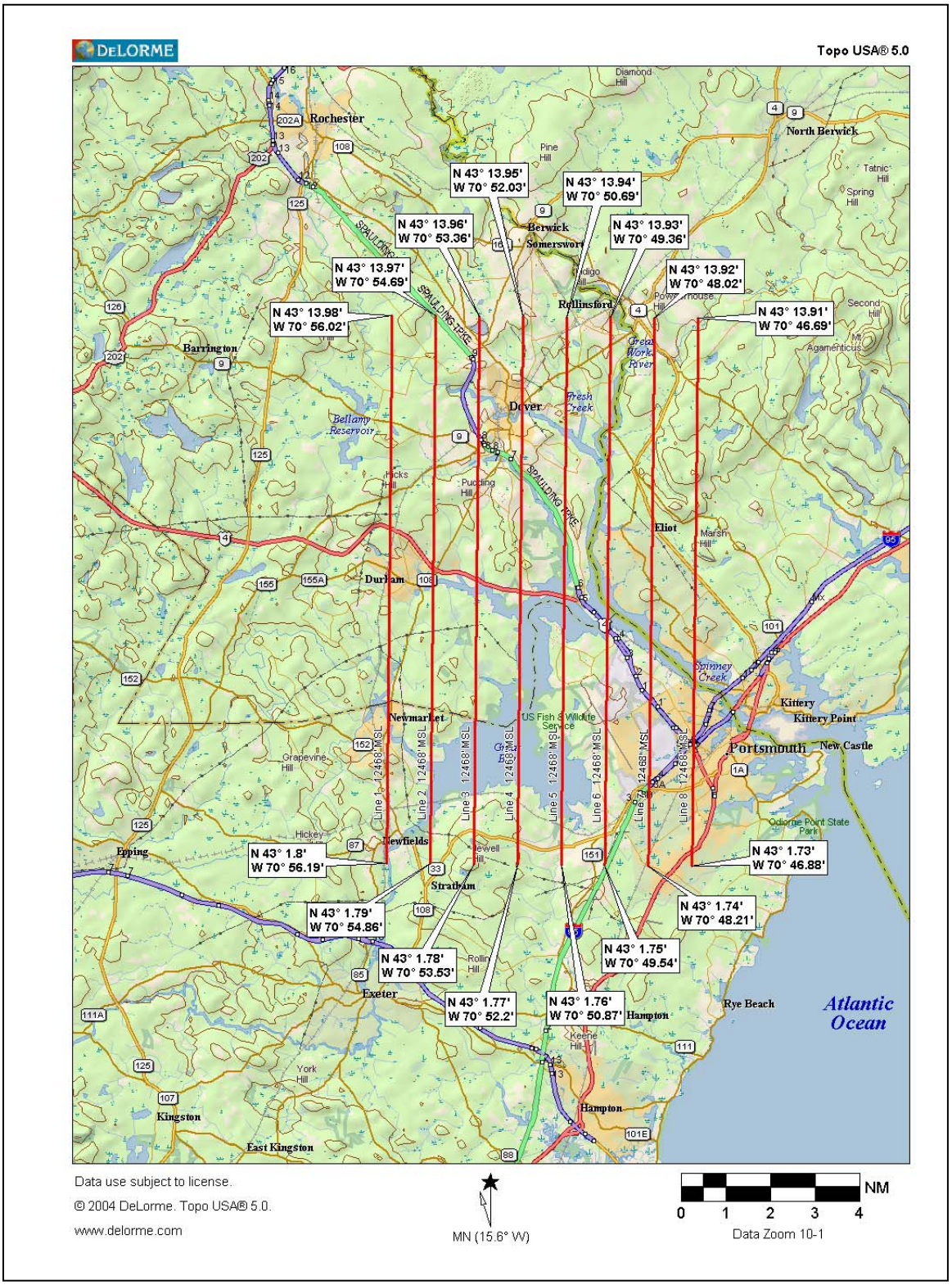

Figure 7.1 Schematic flight-line plan of the Great Bay Estuary hyperspectral survey. The start point and end point are shown in WGS-84 geographic coordinates and the altitude in feet (SpecTIR, 2007).

7.2. Preprocessing

7.2.1. Radiance processing

Radiometric calibration by SpecTIR was achieved through the use of a Labsphere USS-2000-V uniform source. This 20-inch diameter integrating sphere was equipped with three internal 45 watt and one 75 watt externally mounted halogen light sources. Each lamp was powered by separate DC regulated constant current power supplies and the addition of a variable attenuator provided even more precise control of light levels. Luminance output was variable from 0 to 4000 foot-lamberts and measured uniformity was > 98% over the entire 8-inch exit port. This sphere carried a NIST traceable spectral radiance calibration from 400 nm to 2500 nm at a sampling interval of 10 nm. The resultant calibration allowed SpecTIR to provide data that was theoretically within +/- 5% of absolute radiance. However, problems were associated with the calibration at blue wavelengths (see Appendix 11.2).

Wavelength calibration was generated and monitored through a characterized Mercury-Argon (HgAr) emission lamp source. HgAr lamps are a common spectral calibration source for spectrometers and provide several fine distinct emission lines in both the VNIR and SWIR spectral domain allowing for accurate wavelength mapping. During processing, flight data QA/QC procedures relied on well documented atmospheric features such as the Oxygen fraunhaufer line at 760 nm to ensure that accurate wavelength mapping was maintained.

Dark current measurements were included at the end of each flight line. The first step of processing was to remove the dark current “signal” from the imagery. The calibration gain file was then applied to convert the raw data values to radiance units.

7.2.2. Atmospheric correction

The radiances provided by SpecTIR were those collected at the sensor which included both surface and atmospheric components. The TAFKAA atmospheric correction package was incorporated into the ENVI processing software and used to remove the atmospheric component and calculate the surface remote sensing reflectance (Gao et al. 2000; Montes et al. 2001). A spatially consistent atmosphere for the times of data collection was assumed as the wavelength range did not include SWIR channels necessary for the aerosol determination mode in turbid waters.

For the August 29th data collection the ozone content was set to 289 atm-cm (289 DU, data from NASA Ozone processing team, TOMS). Water vapor content (2.3 cm) and aerosol properties (aerosol optical depth of 0.17) were obtained from the Aeronet-processed Thompson farm Cimel Sun photometer operated by the UNH AIRMAP group. Other atmospheric gases were left as default including NO2 which has a column value of 5 x 1015 molecules.

Results from the atmospheric correction and other evaluation procedures for the hyperspectral aerial information indicated that there were problems with data in the blue wavelengths. This was ultimately confirmed by the contractor so only information with wavelengths of 555 nm or above were suitable for the further analysis (further details of

the atmospheric correction and quality evaluation procedures are available in Appendix 11.2).

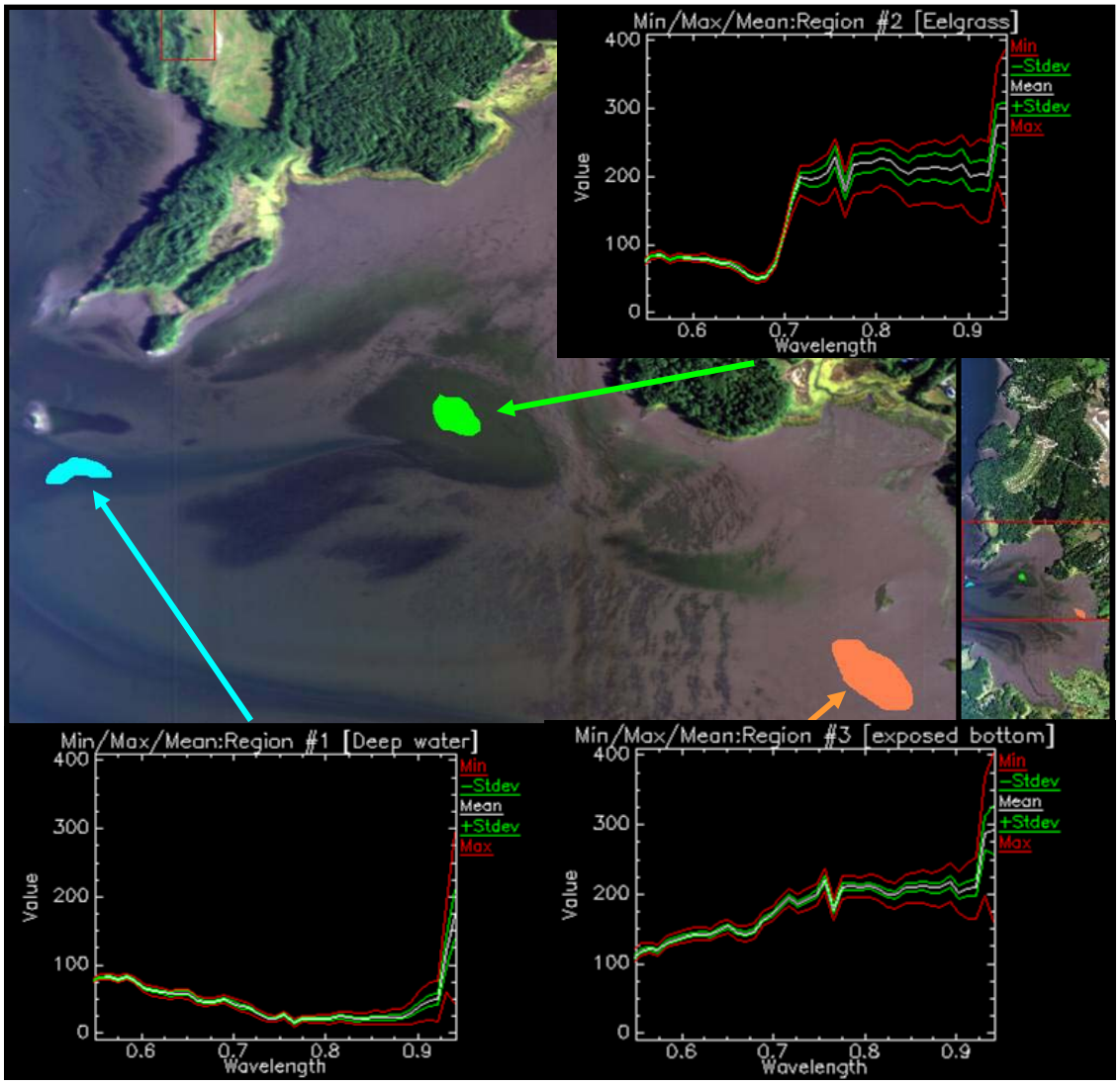

Figure 7.2 Spectral analysis of the pixel-value distribution in Great Bay, NH as a function of wavelength including the mean, minimum (min), maximum (max), and the standard deviation (+/- stdev) values. The three ROIs presented are: 1) Deep water (no bottom contribution), 2) eelgrass bed, and 3) exposed bottom.

7.3. End-member collection

A spectral signature collected from a hyperspectral dataset that represents a spectrally "pure" feature (e.g, vegetation, soil, etc.) is defined as a spectral end-member. Regions of Interest (ROI) containing similar underwater features were identified. Spectral analysis of the value distribution as a function wavelength was conducted for each ROI. Figure 7.2 shows the pixel distribution values of three ROIs: 1) Deep water (no bottom

contribution), 2) eelgrass bed, and 3) exposed bottom. It seems that all the exposed bottom regions contain chlorophyll pigments. This conclusion is based on the spectral characteristics produced from the analysis. The end-members collected were analyzed and aided in construction of decision rule for eelgrass/macroalgae classification. In the following sections only the mean value of the end-member (ROI spectra) and presented.

7.4. Submerged area isolation

The hyperspectral (HS) imagery contained information not only on the waters of the Great Bay Estuary but also of the surrounding watershed. The first task in processing the HS imagery was therefore masking out the land pixels. This procedure is required in order to avoid similar features in the surrounding watershed (such as other water bodies or similar sand) to be classified in the next processing steps. The unsupervised classification was applied to each line (20-25 classes with a change threshold of 3.5%). The resulting output is a hyperspectral image that contains null values in all areas surrounding Great Bay Estuary (example in Figure 7.3)

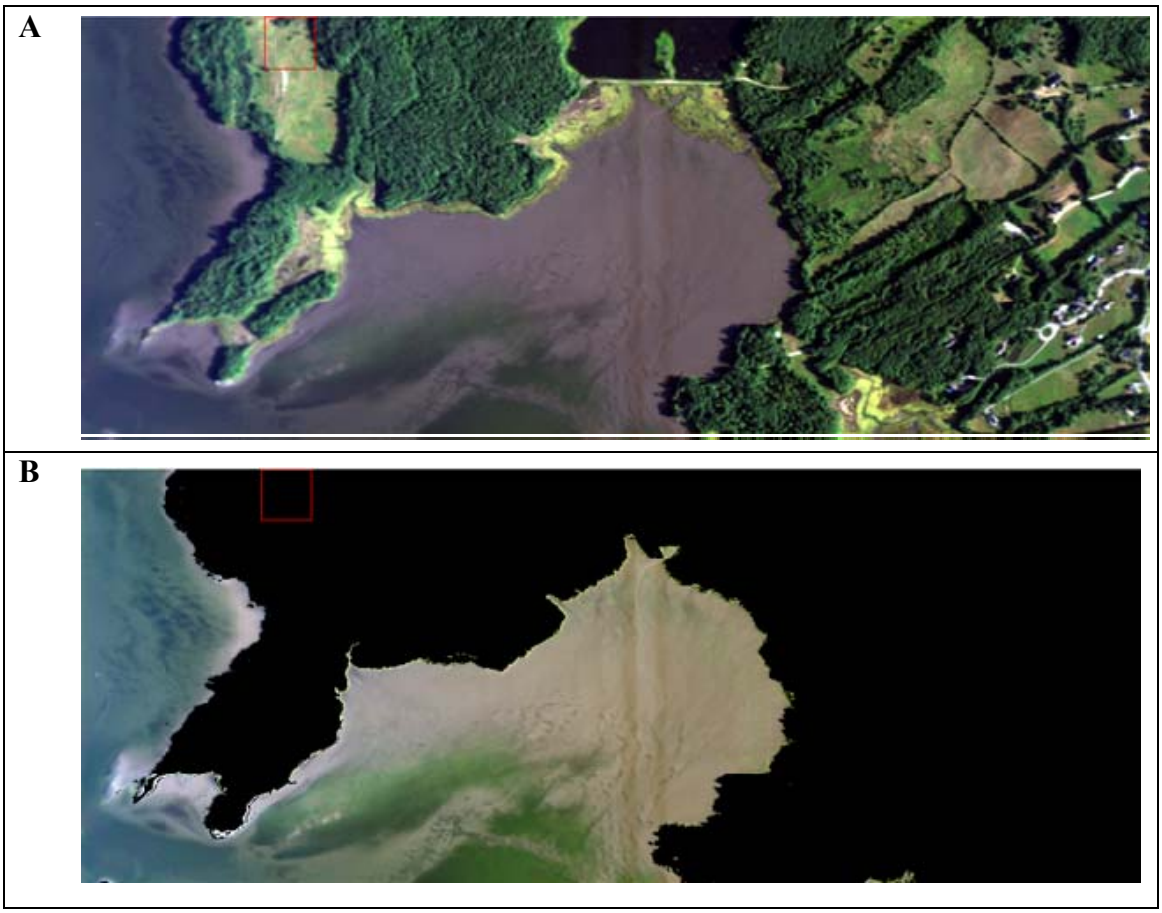

Figure 7.3 Hyperspectral imagery (line 0829-0545) of Herods Cove (Northeast Great Bay) before (A) and after (B) masking out the land pixels of the surrounding watershed areas.

7.5. Vegetation isolation

Four ROIs were used for the vegetation isolation (Figure 7.4.): macroalgae, eelgrass, exposed bottom, and deep water. The maximum separation between the vegetation (macroalgae and eelgrass) and the non-vegetation areas was found using the 0.670 µm and the 0.717 µm channels. This was expected from areas containing the chlorophyll pigment that is characterized with a sharp elevation in reflectance value from 0.660 µm to 0.690 µm that peaks around 0.710 µm to 0.730 µm (section 5.3.). These characteristics are also found in the exposed-bottom ROI, where the value range between the 0.670 µm and the 0.717 µm channels is smaller than the macroalgae and eelgrass ROIs. This indicates that the exposed bottom is composed not only from non-vegetation materials, but also contains some chlorophyll. It is important to note that the chlorophyll trace in exposed-bottom ROI might be suspended in the water column and not resting on the bottom.

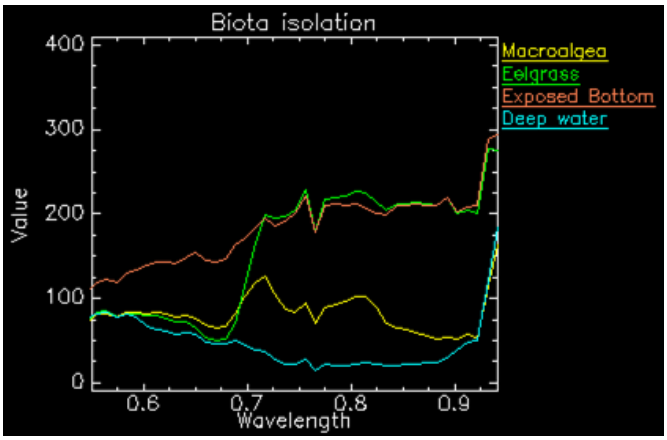

Figure 7.4 (A) ROIs overlaid on the hyperspectral imagery (line 0829-0545): macroalgae (yellow), eelgrass (green), exposed bottom (brown), and deep water (cyan), and (B) the produced end-members of each ROI, respectively.

The algorithm type used for the vegetation isolation was a normalized difference vegetation index (NDVI):

$$NDVI_{biota\_isolation} = \frac{R_{rs}(717) - R_{rs}(670)}{R_{rs}(717) + R_{rs}(670)}$$

where, R_{rs} is the remote sensing reflectance and the channel values are in nm.

Figure 7.5 shows the NDVI-algorithm results. The bright areas in figure 7.5.A represent higher concentration of chlorophyll pigment. Two problems were noticed from the results from the vegetation isolation. The first issue was that there is wetland vegetation is in the data set. The contribution wetland vegetation is noticed in the NDVI-result image as bright regions along the edges of the masked image. The second issue was that water was significant enough to cause attenuation on the bottom reflectance. This issue can be noticed in the bright areas gradually becoming darker towards the channel (figure 7.5.A) and also from the decreasing horizontal-value profile toward the channel (Figure 7.5.B).

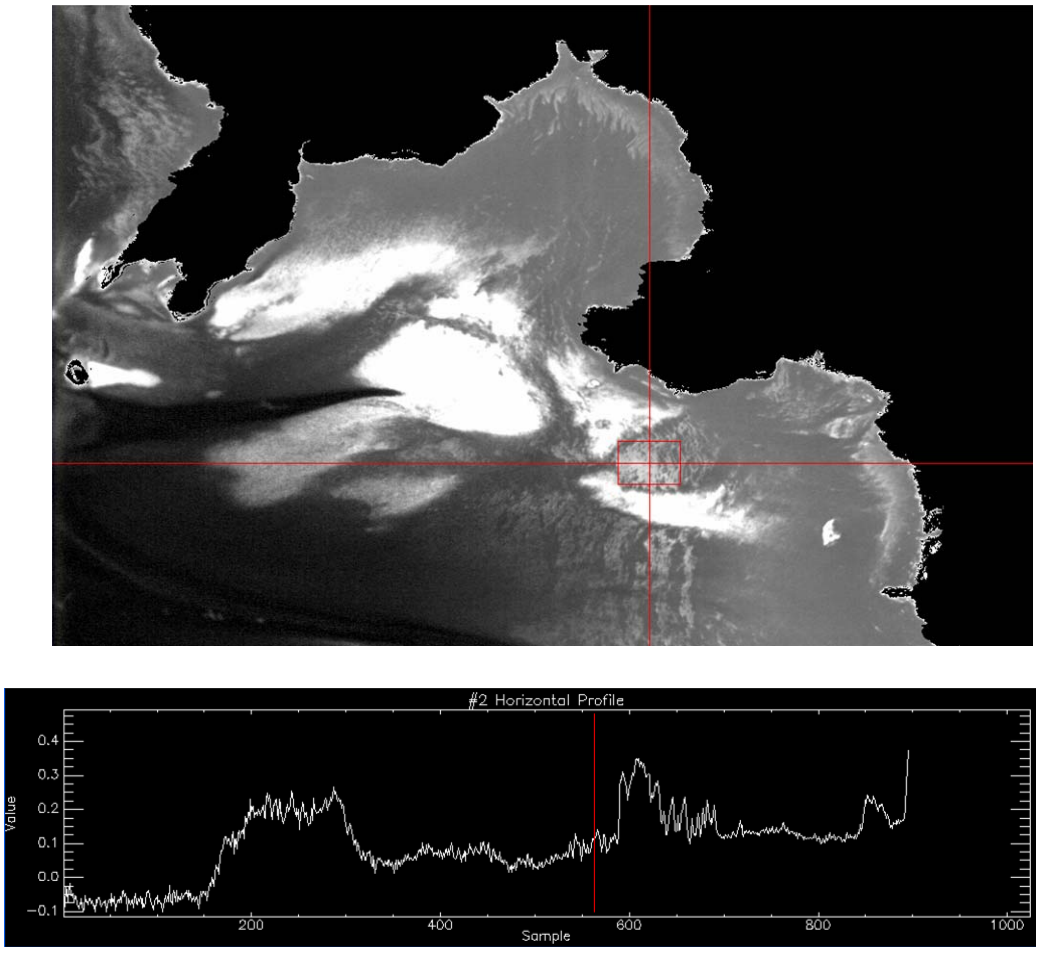

Figure 7.5 Vegetation isolation results: A) result image using the NDVI algorithm; B) Horizontal-value profile from the NDVI image. Brighter areas represent higher concentration of chlorophyll pigment.

7.6. Wetland isolation

Additional end-members representing the wetland vegetation (such as, *Spartina alterniflora*) were collected (Figure 7.6A). A comparison between the wetland vegetation and the eelgrass/macroalgae beds showed a difference in spectra between 0.717 µm and 0.755 µm. Two methods were used for separation: NDVI and Spectral Angle Mapping (SAM). Both methods showed similar results. The best results achieved using NDVI with the 0.717 µm and 0.726 µm (Figure 7.6B).

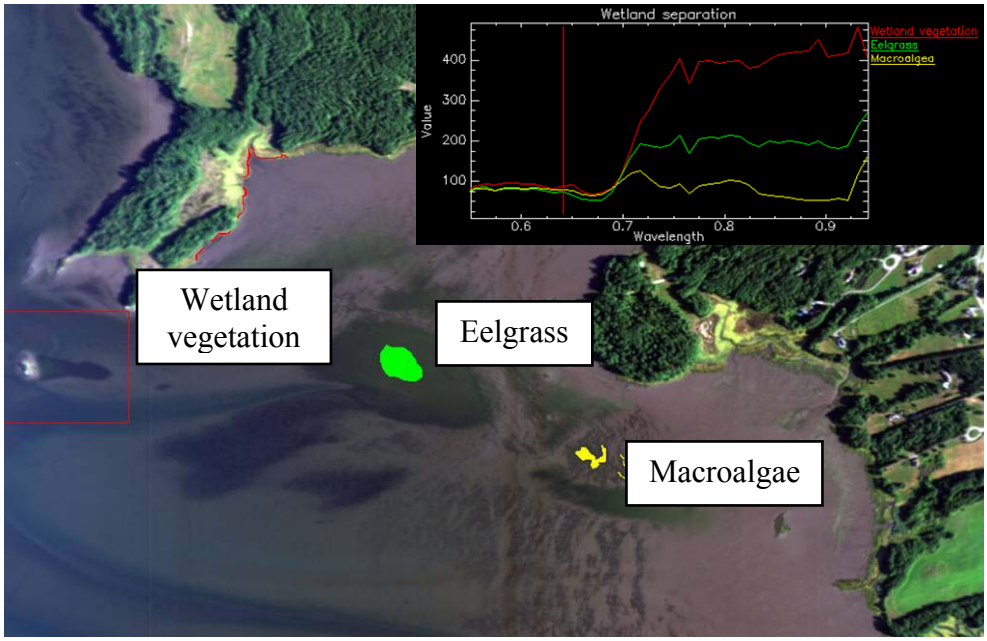

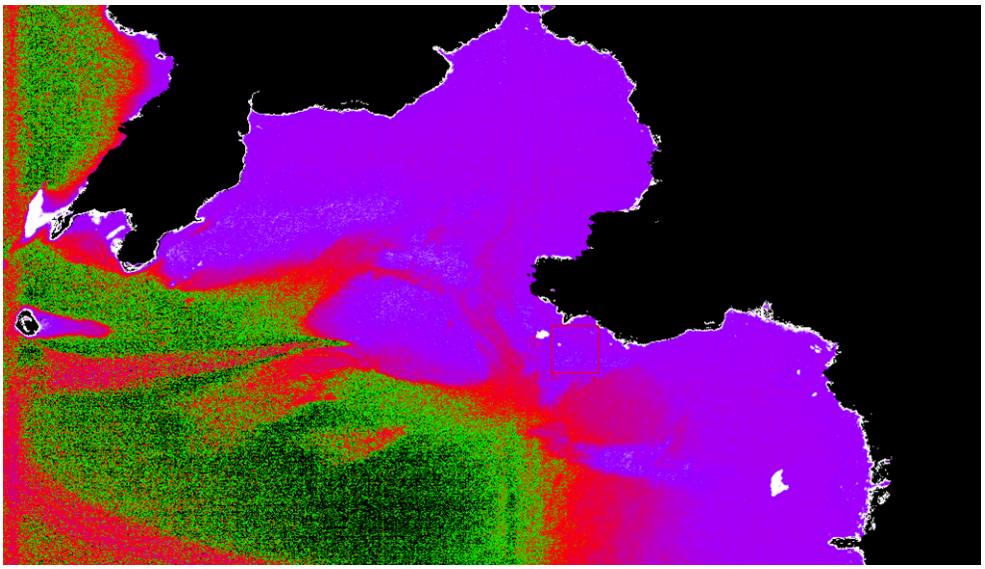

Figure 7.6 Wetland vegetation masking: A) ROIs overlaid on the hyperspectral imagery (line 0829-0545): macroalgae (yellow), eelgrass (green), and wetland vegetation (red) and the produced end-members of each ROI, respectively; B) result image using the NDVI algorithm (without vegetation removal). The white areas in the result image represent the wetland vegetation areas.

7.7. Eelgrass and macroalgae classification

Due to the lack of spectral measurement of eelgrass and macroalgae at the time of the survey, it was decided to focus on identifying and classifying the eelgrass and macroalgae beds. The test site used was eastern Great Bay (line 0829-0545) and the results were checked on sites identified in western Great Bay (line 0829-0604) using expert opinion. End-members were collected from eelgrass and macroalgae ROIs at different depth (Figure 7.7). A comparison between the two groups showed a difference in two spectra regions: 1) 0.574 µm to 0.630 µm, and 2) 0.717 µm to 0.755 µm.

The spectral difference is more noticeable in the 0.717 µm to 0.755 µm range between eelgrass and macroalgae in shallow waters (when the eelgrass canopy is shallower than 0.1 m from the surface). This can be noticed in the end-member comparison in Figure 7.8. Unfortunately, due to the lack of water clarity in the region, the spectra received from eelgrass beds in greater depths (eelgrass canopy is deeper than 0.1 m from the surface) were very similar to the macroalgae beds (figure 7.9).

The spectral difference in the 0.574 µm to 0.630 µm range is more subtle, but it is still noticed at greater water depths. Depth correction is required in order to distinguish between macroalgae and eelgrass in depths greater than 0.1 m. This depth correction was done manually due to a lack of an accurate digital elevation model (DEM) in Great Bay (Appendix 11.3).

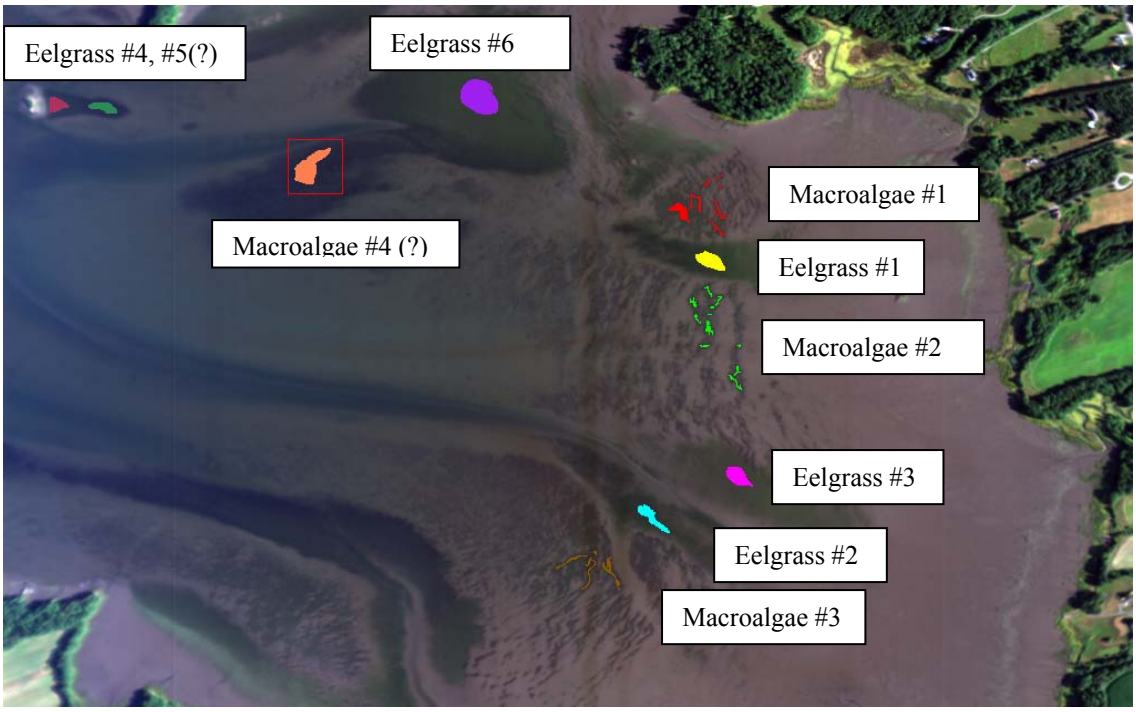

Figure 7.7 Eelgrass and macroalgae ROIs overlaid on the hyperspectral imagery (line 0829-0545).

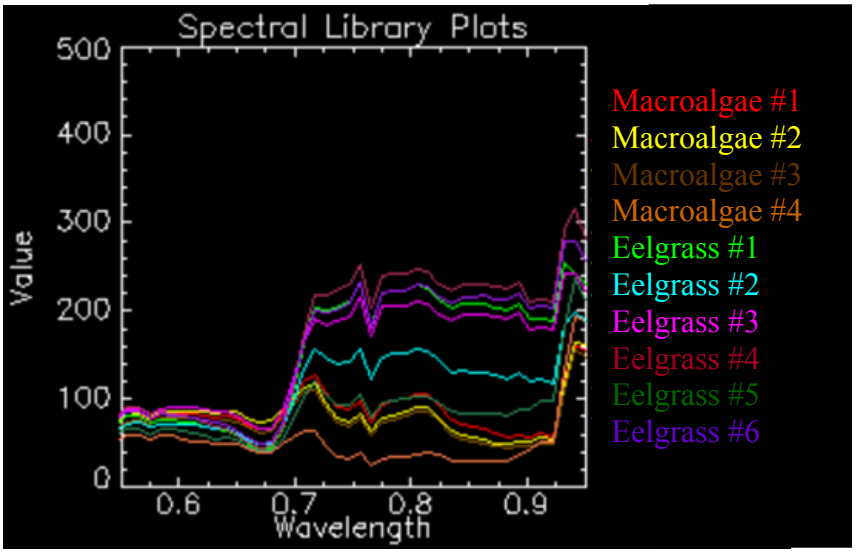

Figure 7.8 Plot of the end-members produced from eelgrass and macroalgae ROIs in figure 7.7.

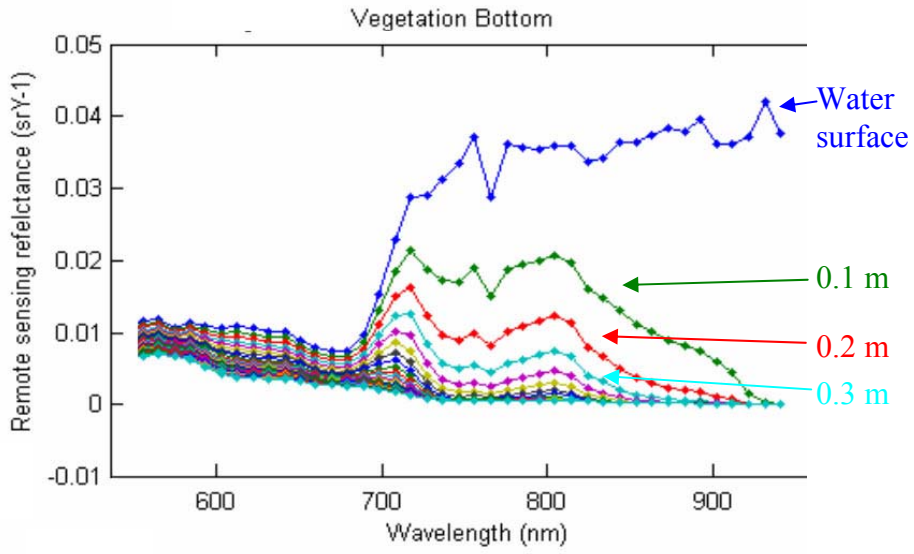

Figure 7.9 Plot of the eelgrass end-member as a function of water depth. Eelgrass beds that have canopy at water depth of 0.2 m and deeper will produce a reflectance spectra similar to macroalgae in the 0.717 µm to 0.755 µm wavelength range (Figure 7.8.).

7.8. Georeferencing

The resulting class files are in image space (no attitude corrections or referencing to a known datum). Input geographic lookup tables (GLTs) that were provided by SpecTIR were used to georeference the class files to WGS-84 datum with a UTM projection (Zone 19N). The georeferenced images have null values around their edges. This is required for merging the class files together.

After georeferencing of the class files, all 8 individual class files (one class file per line) were merged into a single file. Aircraft attitude (yaw, pitch, and roll) can be noticed at the edges of the georeferenced image.

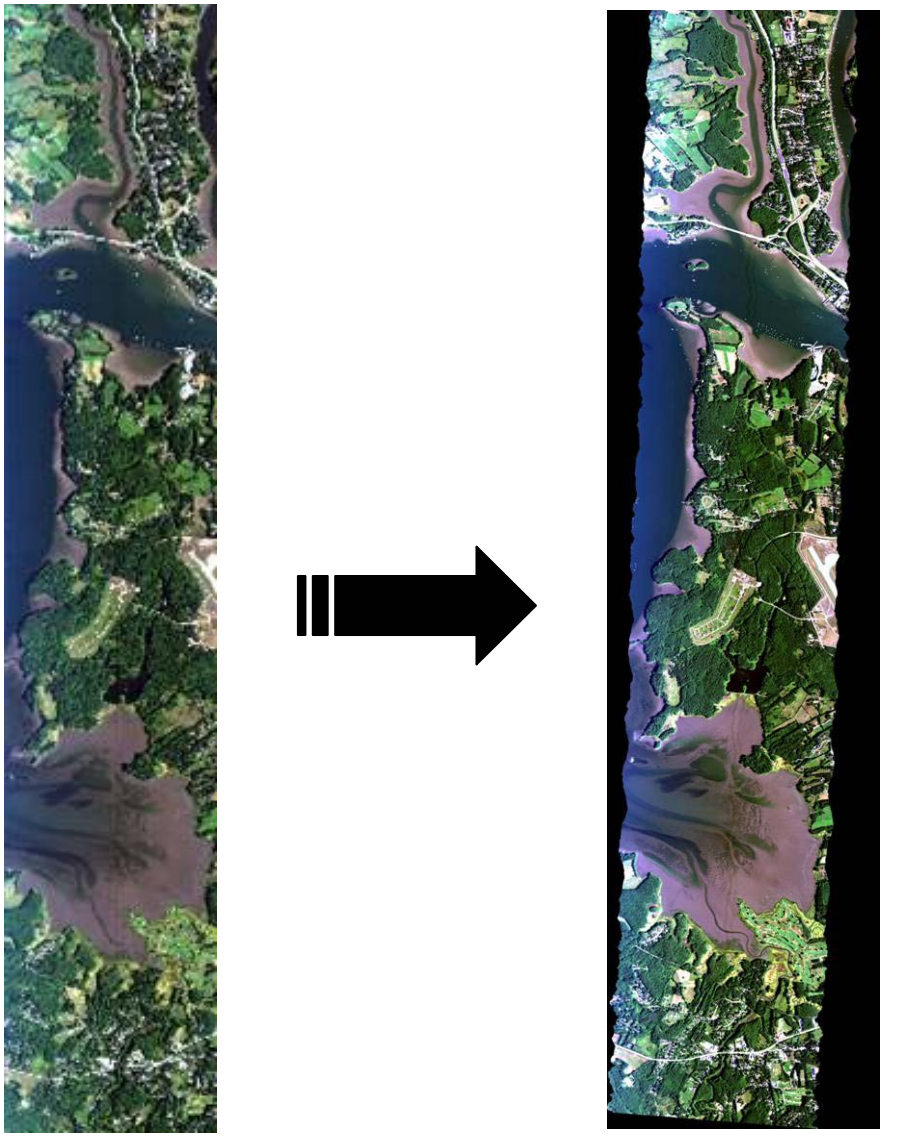

Image space **Georeferenced to a datum**

Figure 7.10 Georeferencing line 0829-0545. The line is projected from image space (X,Y) into a known datum (latitude and longitude or easting and northing).

7.9. Data export (ArcMap shapefile format)

The ENVI class files were exported to an ArcMap-polygon shapefile, which shapefiles were subset into the NHDES estuary assessment zones (Figure 7.11). All files were georeferenced in WGS-84 UTM (zone 19) and New Hampshire State Plane NAD 1983 (FIPS 2800).

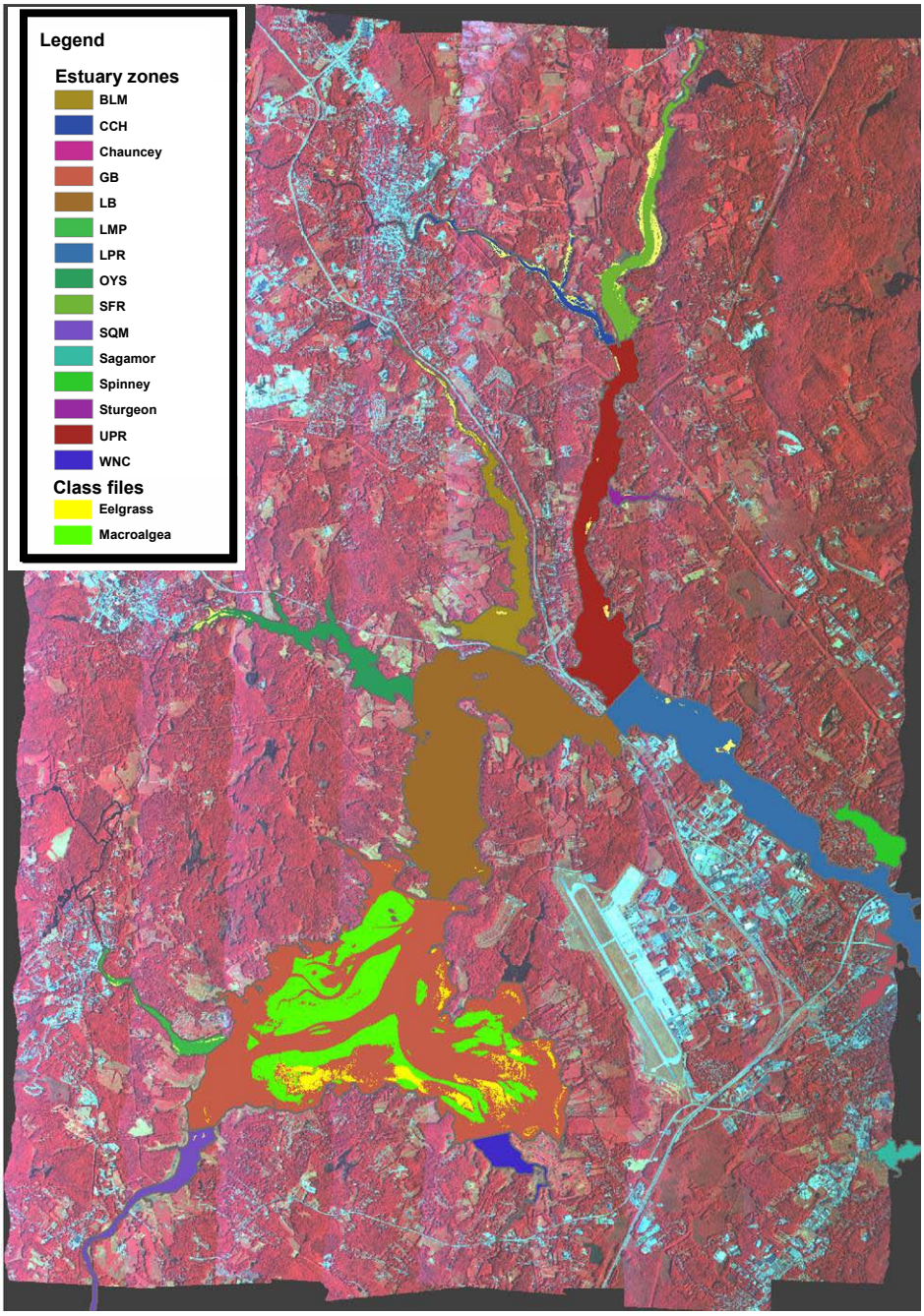

Figure 7.11 Overview map of Great Bay Estuary hyperspectral project 2008 with the NHDES estuary assessment zones color coded and the eelgrass and macoalgae beds.

8 Results and Discussion

8.1. Eelgrass and macroalgae mapping procedure based on the AISA hyperspectral remote sensing imagery

The procedure developed for macroalgae and eelgrass mapping based on AISA hyperspectral imagery from the 2008 survey (Figure 8.1) is as follows:

1) The hyperspectral dataset at the reflectance level should undergo a quality assurance (QA) before processing. The QA will include inspection of sprectra received from known features in hyperspectral dataset to spectra from field measurements or a spectral library.

2) In case the QA results from the reflectance level are not good, an atmospheric correction processing should be applied to the dataset at the radiance level (e.g., TAFKAA). This is assuming the dataset at the radiance level is good.

3) The water body is isolated from the surrounding areas. This is done by applying unsupervised classification on the dataset and selecting the classes containing the water body. The selected classes are then merged and are used to mask the surrounding areas.

4) The vegetation is separated from the exposed bottom and the deep water using the 0.670 μm and 0.717 μm channels.

5) Wetland and land vegetation that is found at the edges of the isolated vegetation dataset is separated using the 0.717 μm and 0.726 μm channels.

6) The final stage classifies the remaining pixels to macroalgae and eelgrass using the 0.574 μm to 0.630 μm channels, and with the input of expert opinion. Depth correction is required for a applying successful classification algorithm.

7) The resulting class files are georeferenced using geographic lookup tables (GLTs).

8) The georeferenced class files are exported into ArcMap polygon shapefiles and are subset to the NHDES estuary zones.

It is important to note here, that this procedure is not a robust automatic procedure and it requires the operator's interaction and guidance of experts on macroalgae and eelgrass in the field. Also, this procedure is adequate to the specific data set of this study and more work with the guidance of experts is required for increased accuracy in image detection.

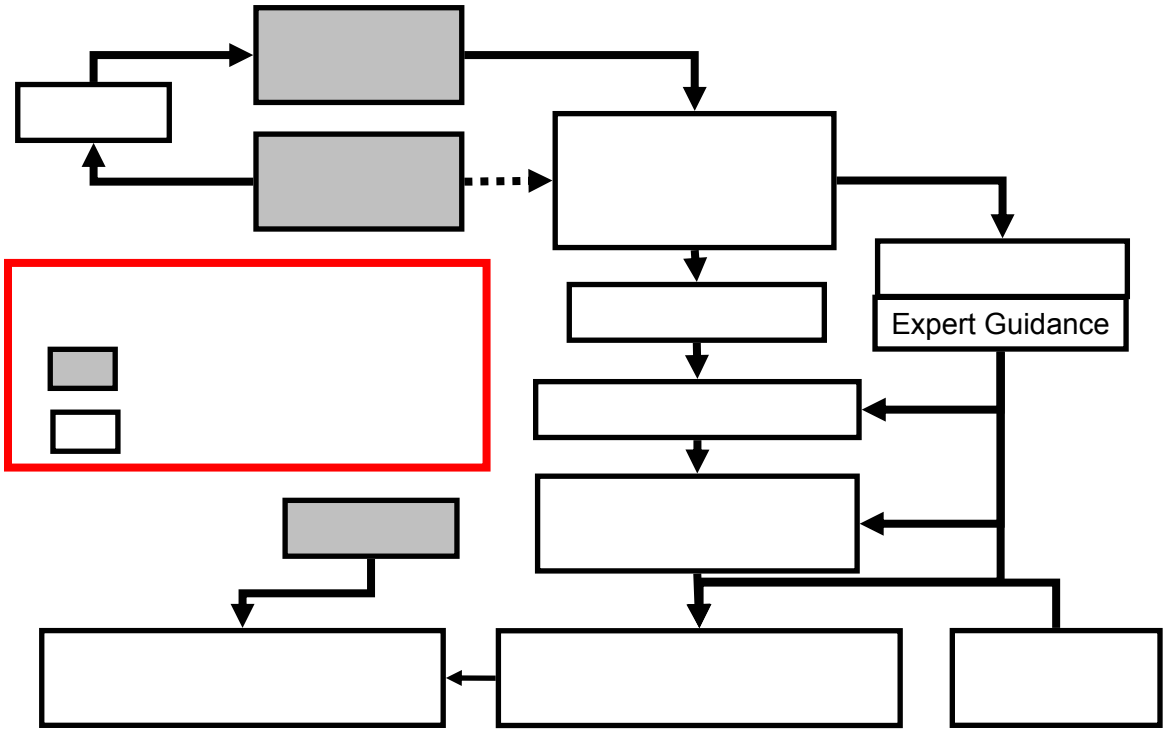

Figure 8.1 Flow chart for eelgrass and macroalgae mapping using the AISA hyperspectral dataset.

8.2. Eelgrass and macroalgae maps using data collected from 2008 NHDES hyperspectral survey

8.2.1. NHDES hyperspectral survey 2008

Two hyperspectral missions were flown with replicate 8 lines of data collection oriented approximately north-south. On August 29 the center time for the central line over Great Bay was 08:57 local time (12:57 GMT) and on October 17 the center time for the same line was 14:11 local time (18:11 GMT). Conditions on August 29 were near perfect with nearly cloud free skies and a low tide at the Squamscott Railroad Bridge predicted for 08:49. The plan to coincide the second mission in October with the time of high tide was complicated by availability of the aircraft and sensor. A compromise time for a low tide of 12:03 on October 17 was chosen. Unfortunately heavily overcast conditions at the departure airport delayed the hyperspectral flight approximately two hours. The weather conditions were not quite as perfect as the previous collection period with some being clouds apparent.

8.2.2. Data quality and atmospheric correction

A variety of techniques were used to assess the quality of the remotely sensed data. A Tafkaa atmospheric correction and other methods that are detailed in Appendix 11.2 concluded that there were large uncertainties associated with wavelengths less than approximately 0.550 µm. Recent communication from SpecTIR, the contractor for the aerial imagery, indicated concerns with the radiometric calibration at these blue wavelengths. Mapping of eelgrass and macroalgae is possible above 0.550 µm, but more advanced classification, such as macroalgae type, requires information below 0.550 µm (Haxo and Blinks 1950). As such, we were unable to classify the macroalgae type. Given the time constraints associated with funding available for the work, only the overflight on August 29, 2007 was able to be analyzed.

8.2.3. Eelgrass and macroalgae distribution as a function of NHDES Estuary assessment zones

The eelgrass and macroalgae distribution results from the August 29, 2007 survey are summarized in Table 8.1. Macroalgae digital signatures on the hyperspectral image were based on interpretation for Great Bay only; additional macroalgae occurring in other parts of the GBE were not specifically assessed and the values in Table 8.1 are an underestimate of total macroalgal abundance in the estuary. The small eelgrass areas in Little Bay and the Piscataqua River in 2007 were not detected in the HS imagery.

Table 8.1 Eelgrass and macroalgae distribution as a function of NHDES Estuary assessment zones

Zone	Macroalgae (Acres)	Macroalgae (M^2)	Eelgrass (Acres)	Eelgrass (M^2)
Great Bay (GB)	207.75	765,578	1158.94	4,690,081
Little Bay (LB)	0.67	2700	0	0
Squamscott River (SQM)	0.76	3050	0	0
Winnicut River (WNC)	0	0	0	0
Bellamy River (BLM)	17.38	70,324	0	0
Chocheco River (CCH)	37.78	156,949	0	0
Lamprey River (LMP)	6.31	25,540	0	0
Oyster River (OYS)	13.31	53,894	0	0
Upper Pistaqua River (UPR)	7.66	31,008	0	0
Lower Pistaqua River (LPR)	8.90	36,035	0	0
Salmon Falls River (SFR)	60.71	245,682	0	0
Sturgeon Creek (Sturgeon)	0.59	2400	0	0

Expert guidance (Drs. Fred Short and Art Mathieson) helped to outline the variety of macroalgae, wetland vegetation and eelgrass distribution and identify locations where vegetation patches are not mixed and contain only one type of vegetation. The resulting mapping product is presented in Figure 8.2.

Figure 8.2 Eelgrass (green) and macroalgae (yellow) distribution overlaid on the survey project mosaic.

8.3. Recommendations

Recommendation for planning future hyperspectral surveys are provided in section 10.

9 Conclusions

A final version of the process was configured after several interactions with eelgrass and macroalgae experts. Additional end-members were identified in the hyperspectral dataset (such as wetland vegetation). Also, the expert guidance aided in the algorithm threshold selection according to the resulting spatial distribution of the class. The final results of the process showed good results that correlate with independent manual analysis of the experts for eelgrass; however, macroalgae in the Great Bay was not fully detected with the final process and additional guidance is needed to capture the complete macroalgal groups.

Without reference spectra of eelgrass and macroalgae and a detailed DEM of the estuary, it is hard to resolve between eelgrass and macroalgae in the inferred vegetation areas. This is mainly to the water attenuation that affects the reflectance as a function of depth. Manual segmentation is able to provide a partial solution, where the depth location is subjective to the operator's decision.

10 Recommendations (for future work or management strategies)

This work together with associated work on the spatial distributions of eelgrass and macroalgae in the Great Bay Estuary has highlighted the potential of HS aerial imagery for management of coastal waters. However, eelgrass and macroalgae mapping was limited due to the complexities associated with the inclusion of remotely detectable bottom reflection underwater. Three major issues that can improve the classification results and allow more advance applications, such as identification of macroalgae types are: conducting more ground truth measurement at the time of the HS survey, acquiring current DEM model of GBE, and examining additional HS datasets with expert guidance. As yet, it is not possible to fully distinguish all eelgrass and macroalgal beds using HS imagery and mixed areas of the two are problematic. Also, without the DEM model the deep edge of the eelgrass beds is not always clearly delineated. Further work should include:

Ground truth measurements- Field measurements of the reflectance spectra are highly valuable for QA of the dataset, applying water depth correction to the dataset, and constructing decision rules for classification. The field measurements should be conducted at the time of the HS survey (up to a few days before or after the survey). A comparison of the field measurements to the HS dataset will provide information if a correction is required. Also, the spectral change as a function of water depth can be investigated. A comparison between the different features (e.g., eelgrass, different types of macroalgae, wetland vegetation, and exposed bottom) will allow identifying spectral

characteristics of the different features for producing more accurate decision rules for classification in the future.

Digital elevation model of the Great Bay Estuary- The existing elevation model of Great Bay Estuary does not contain accurate and high resolution bathymetry. A more updated elevation model that also covers the shallow areas, especially in Great Bay, is required. The bathymetry will allow correcting the HS dataset attenuation at different water depths. This will provide classification products that can be more accurate (spatial coverage in deeper water depths).

Examination of additional HS datasets with expert guidance- It is recommended to examine additional HS datasets on the same survey area and also to investigate sites near the mouth of the GBE (Portsmouth Harbor). Environmental conditions may vary in location and at different seasons that may affect the procedure configuration. It is also recommended that this work should be done with expert guidance on vegetational types and possible scenarios for change in the environmental conditions.

Uncertainties associated with water depth and the inversion of the HS imagery could be further decreased if concurrent HS imagery and LIDAR information can be fused together. Such data has already been collected for the mouth of the Great Bay Estuary / Portsmouth Harbor where additional eelgrass beds exist. This data could provide valuable information of future techniques for remote sensing of water quality and benthic habitat characteristics.

Table 11.1 (top) Flight specs of the NHDES 2008 hyperspectral survey, **(bottom)** Line planning specs for the survey.

Flight Specs	
Spec	**Value**
Focal length	23.1 mm
Pixel size	30 microns
AGL altitude	12497 m
Line velocity	120 knots
GSD	2.5 m
overlap	30 %
Max line offset	0.207 nm

	Flight hieght			Projected (WGS-84)			
Flight line	**Meters**	**Feet**	**f [mm]**	**Line start**		**Line end**	
1	3800	12,468	62.5	70° 56' 11.12" W	43° 1' 47.86" N	70° 56' 1.34" W	43° 13' 58.56" N
2	3800	12,468	62.5	70° 54' 51.55" W	43° 1' 47.35" N	70° 54' 41.50" W	43° 13' 58.04" N
3	3800	12,468	62.5	70° 53' 31.88" W	43° 1' 46.81" N	70° 53' 21.57" W	43° 13' 57.50" N
4	3800	12,468	62.5	70° 52' 12.22" W	43° 1' 46.28" N	70° 52' 1.65" W	43° 13' 56.95" N
5	3800	12,468	62.5	70° 50' 52.45" W	43° 1' 45.71" N	70° 50' 41.61" W	43° 13' 56.39" N
6	3800	12,468	62.5	70° 49' 32.50" W	43° 1' 45.13" N	70° 49' 21.40" W	43° 13' 55.81" N
7	3800	12,468	62.5	70° 48' 12.58" W	43° 1' 44.53" N	70° 48' 1.21" W	43° 13' 55.22" N
8	3800	12,468	62.5	70° 46' 52.81" W	43° 1' 43.93" N	70° 46' 41.17" W	43° 13' 54.59" N

11.2. Quality evaluation of the hyperspectral data set

11.2.1. Introduction

A quality assurance (QA) of the hyperspectral (ASIA) data was done in order to evaluate the AISA dataset. Good QA results would allow processing the data “as is” and bad QA results would require pre-processing procedures or considering a different approach to process the data (instead of processing the data in the reflectance level). The reflectance data inside the water body was problematic for this specific study. There was no spectral information above 900 nm (i.e. the values were the same for all channels between 902 nm and 951 nm, Figure 10.1). In addition, the spectral signatures do not correlate with those of characteristic of estuarine environments available from an historical spectral library or measurements using a field spectrometer.

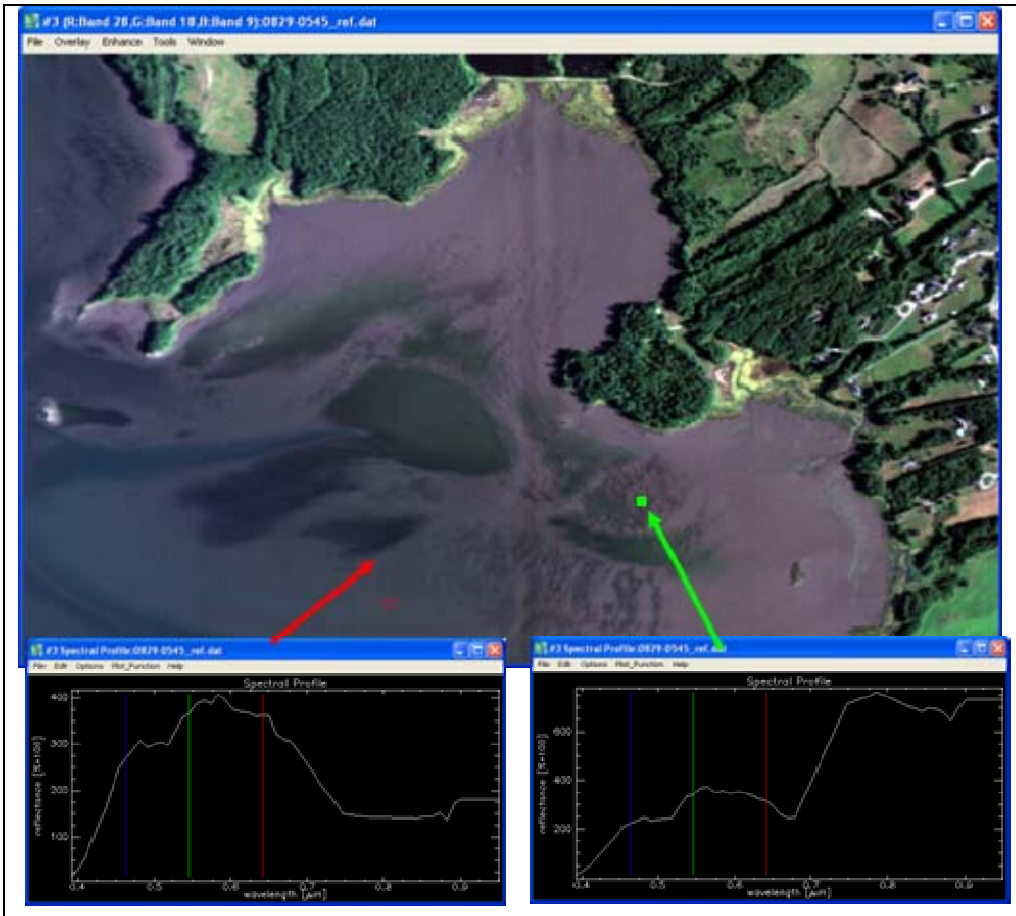

Figure 11.1 Two spectral-signatures bottom two panels from a reflectance-level image with image details in top panel (0829-0545 is the flight line). The spectral signatures on the bottom left (red box in the overview image) is a sandy exposed bottom and spectral signatures on the bottom right (green box in the overview image) is a vegetated bottom

{red box is in the wrong place}

Following these results, an evaluation was conducted on the imagery at a radiance level. The evaluation was conducted in two independent methods: simulated atmospheric model independent from the dataset (MODO) and simulated atmospheric model based on the hyperspectral dataset (TAFKAA). Oxygen mapping test was also conducted on the dataset.

11.2.2. MODO simulation

The MODO (MODTRAN4 Interface) simulation software was used in this study to simulate spectral signatures at a radiance level. The inputs provided are the environmental conditions (sample location, time, and atmospheric condition) and an end-member of interest. The goal of the MODO processing was to produce an independent signature dataset that could indicate the quality of the AISA data.

The methodology used in the MODO simulation was: field measurement of reference targets, simulate synthetic-spectral signatures from the targets collected in the field measurements, and compare between the synthetic-spectral signatures and the signatures from the radiance datasets. These steps are elaborated as follows:

1. Spectral signatures (reflectance) of different targets were collected. The signatures were mainly, sand, gravel, concrete, old (fair colored) asphalt, and new (dark) asphalt (Table 11.2). All signatures were collected around Great Bay (4.3.2008). Asphalt and concrete target are can be considered as ideal QA targets, since their spectral signature does not vary much with time (over a period of months) and can be considered stable.

Table 11.2 Summary table of the spectral signatures collected for the study

Target number	Location	Target measured
Target 1	Dover DMV Parking Lot	Asphalt
Target 2	Newick's Parking Lot	Asphalt Sand Concrete
Target 3	Hilton Park	Gravel Asphalt
Target 4	Northwest Scammel Bridge	Asphalt
Target 5	Durham's New Landing	Sand
Target 6	Durham's Old Landing	Sand
Target 7	Adam's Point	Asphalt
Target 8	New Market's Municipal Parking Lot	Gravel Asphalt

2. Spectral signatures (reflectance) of the different targets were imported into the software.

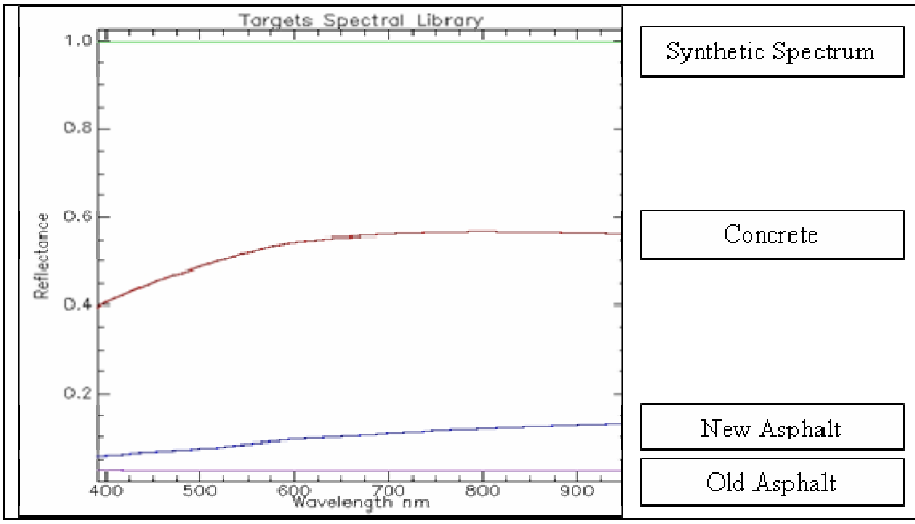

Figure 11.2 Spectral plot reflectance (value of 1 is 100 %) as a function of wavelength of the collected field measurement signatures and of the synthetic spectrum (white reference)

3. The sun geometry was calculated for the time of the HS survey (morning time) and was also calculated at evening for observing spectral changes.

4. The atmospheric conditions at the time of the survey were simulated.

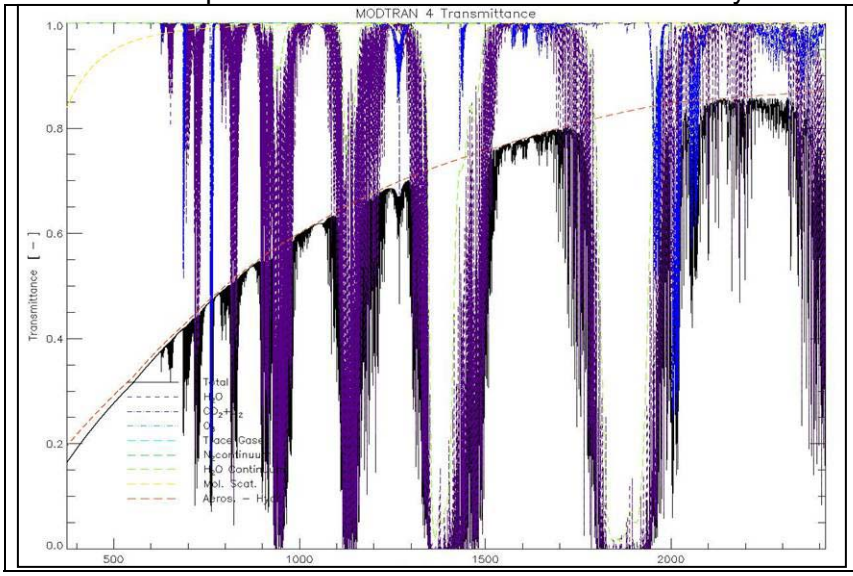

Figure 11.3 Spectral plot of the atmosphere in the transmittance level (transmittance value [%] as a function of wavelength [nm]) at the time of the survey. The black line in the plot represents the atmospheric transmittance.

5. The sensor's radiation as a function of wavelength was simulated based on the atmospheric conditions. The resulting product was a radiance plot (radiance value [W/m2sr·nm] as a function of wavelength [nm]) that can translate the field measurements to radiance values at the time of the survey.

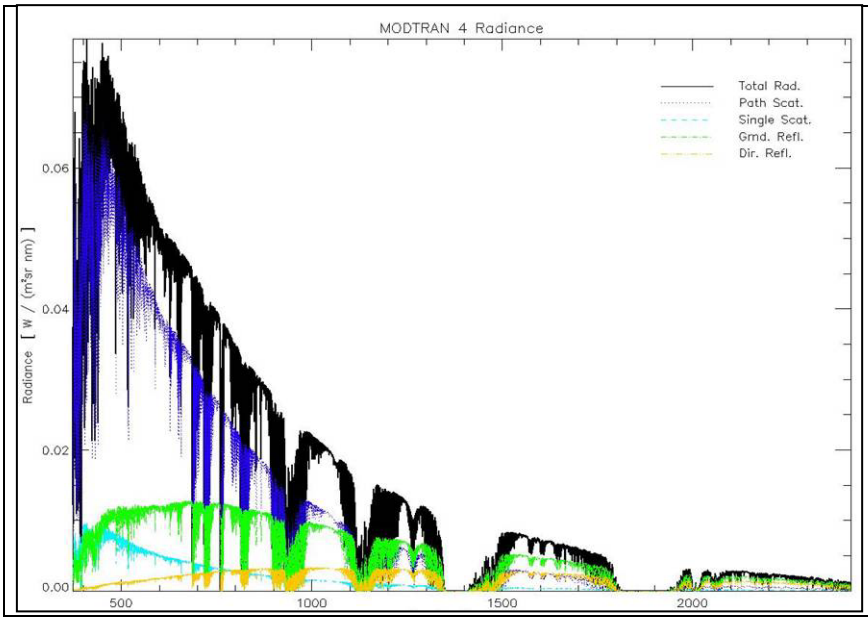

Figure 11.4 The radiance plot (radiance value [W/m^{2}sr·nm] as a function of wavelength [nm]). The black line represents the total radiance.

6. Radiance values for the different targets as a function of wavelength were simulated for morning time at 8:30 local time (blue spectrum) and for the afternoon time at 15:30 local time (red spectrum).

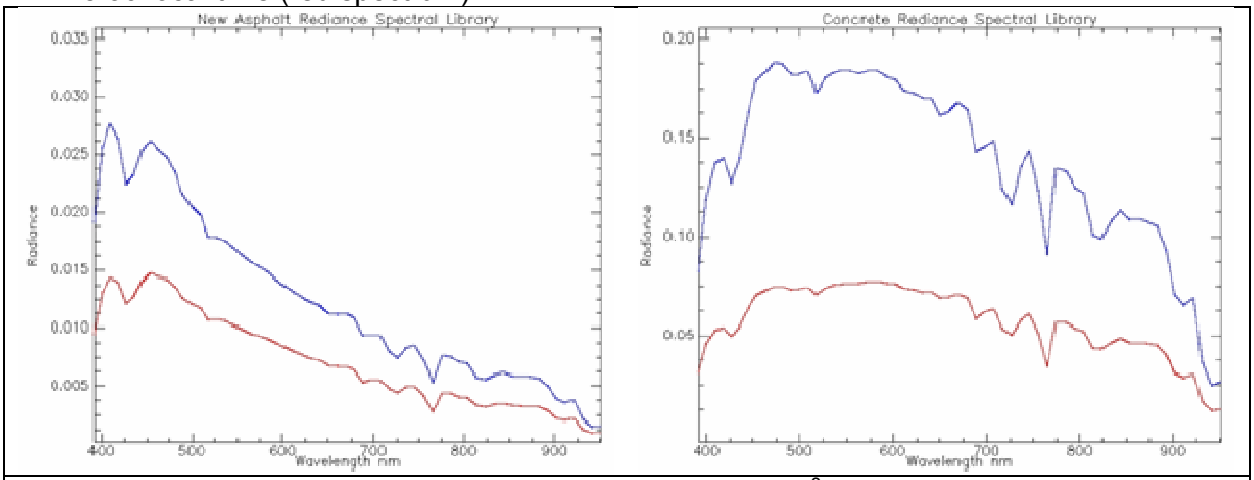

Figure 11.5 Simulated-spectral signatures in radiance [W/m^{2}sr·nm] of two targets measured in the field: new asphalt (left plot) and concrete (right plot). The blue line and the red line are the spectral signatures in radiance level for a morning survey (8:30 local time) and an afternoon survey, respectively.

7. The most prominent results were observed in the comparison of asphalt where a gain value in the blue to green-blue (400 nm to 550 nm) is noticed. The spectral signitured were compared in the radiance level and were also compared after a continuum removal normalization of the radiance values.

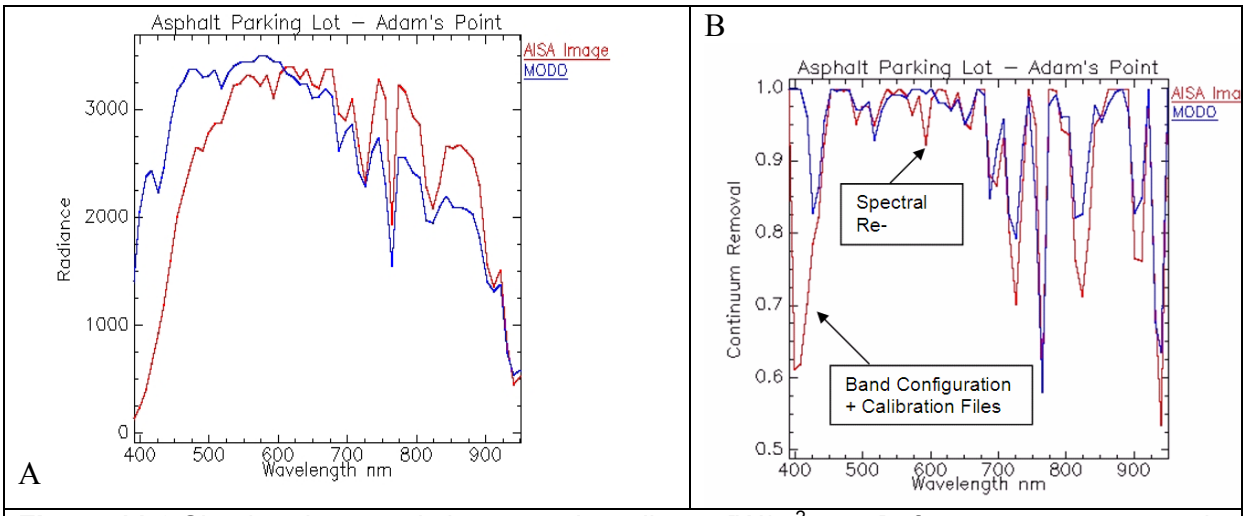

Figure 11.6 Simulated-spectral signatures in radiance [W/m^{2}sr·nm] of two targets measured in the field: new asphalt (left plot) and concrete (right plot). The blue line and the red line are the spectral signatures in radiance level for a morning survey (8:30 local time) and an afternoon survey, respectively.

The results from the MODO simulation showed a good correlation between the spectral signatures of targets sampled from the AISA image and the field measurements in the 570 nm - 800 nm region. The correlation is both on the spectral values and the location of various spectral features along the signature. The correlation of the two datasets in the 400 nm – 550 nm region did not show a good correlation. A gain artifact was noticed that might be caused due to a problem in the band configuration or the calibration files. Also, some spectral features varied between the two data sets. This might be due to a spectral re-sampling.

11.2.3. TAFKAA Atmospheric Correction of SPEC-TIR AISA/Eagle over-flight 08/29/2007

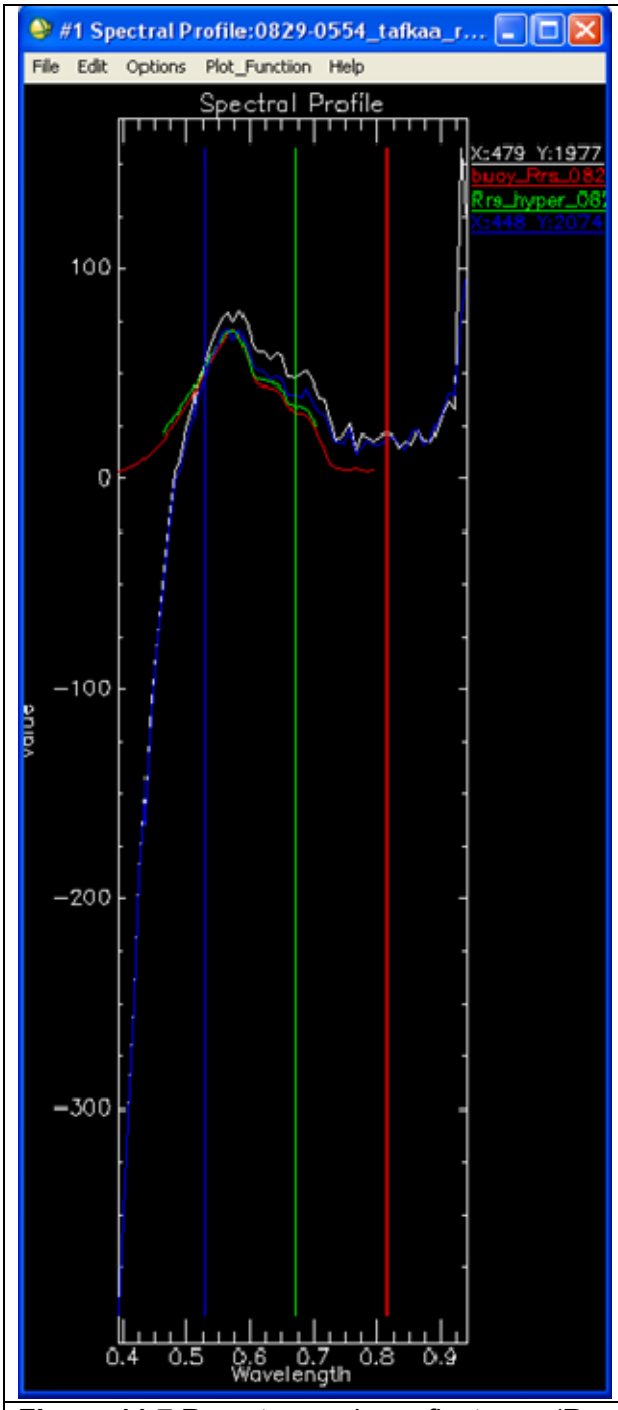

Figure 11.7 Remote sensing reflectance (R_{rs} * 10000) with wavelength. Tafkaa retrieved values (white line) and in-water measurements (red – buoy, green – profiling radiometer). The blue line is a nearby pixel.

The example is for a smaller subset of the main over-flight line that passed overhead of the buoy in Great Bay, NH. The calculated atmospheric correction corrected remote sensing reflectances from the HS over-flight (white and blue lines) were compared to those calculated at the buoy with *in-situ* sensors with hyperspectral sensors (HyperOCR, Satlantic Inc). These included sensors on the buoy (redline on Figure 11.7, surface Es as well as an Lu and Ed pair at ~1m) as well as a submersible profiling radiometer (Hyperpro-II, green line).

The atmospheric correction was performed with Tafkaa – 6S with fixed values for atmospheric components over the whole scene. Tafkaa input files are provided below. Data sources for these values were: Column ozone (289 DU) from NASA Ozone processing team (TOMS). Water vapor (2.3 cm) and aerosol properties (aerosol optical thickness was 0.17) were from the Aeronet processed Thompson farm Cimel Sun photometer. Other atmospheric gasses were left as default including the NO2 which has a column value of 5e15 molecules.

Results: There appears to be good agreement with the spectra above ~ 0.55 microns (550 nm) but below this the HS imagery reflectances (and water leaving radiances) diverge significantly. Three possible causes for this disagreement at lower wavelengths include:

9) Overcorrection for aerosols,
10) High NO2 concentrations with its associated increase

in absorption at wavelengths below 600 nm (high NO2 is associated with atmospheric pollution), or

11) Problems associated with instrument performance / calibration issues at these blue wavelengths.

Three additional Tafkaa runs were performed to assess the possible contribution of the first aerosol overcorrection and NO2 pollution:
1) For aerosol overcorrection the aerosol optical depth was set to zero such that no aerosol correction would be performed (Figure 11.8A). 2) For NO2 pollution the background concentration was increased by a factor of 90. NOy data from the UNH AIRMAP facility at Thompson Farm indicated that there was a potential pollution event at the time (Figure 11.8B). 3) To assess the combined potential impact of the aerosol over correction and NO2 pollution the aerosol optical depth was set to zero and NO2 increased by a factor of 90 (Figure 11.8C). For all three additional atmospheric correction scenarios negative remote sensing reflectances were retrieved.

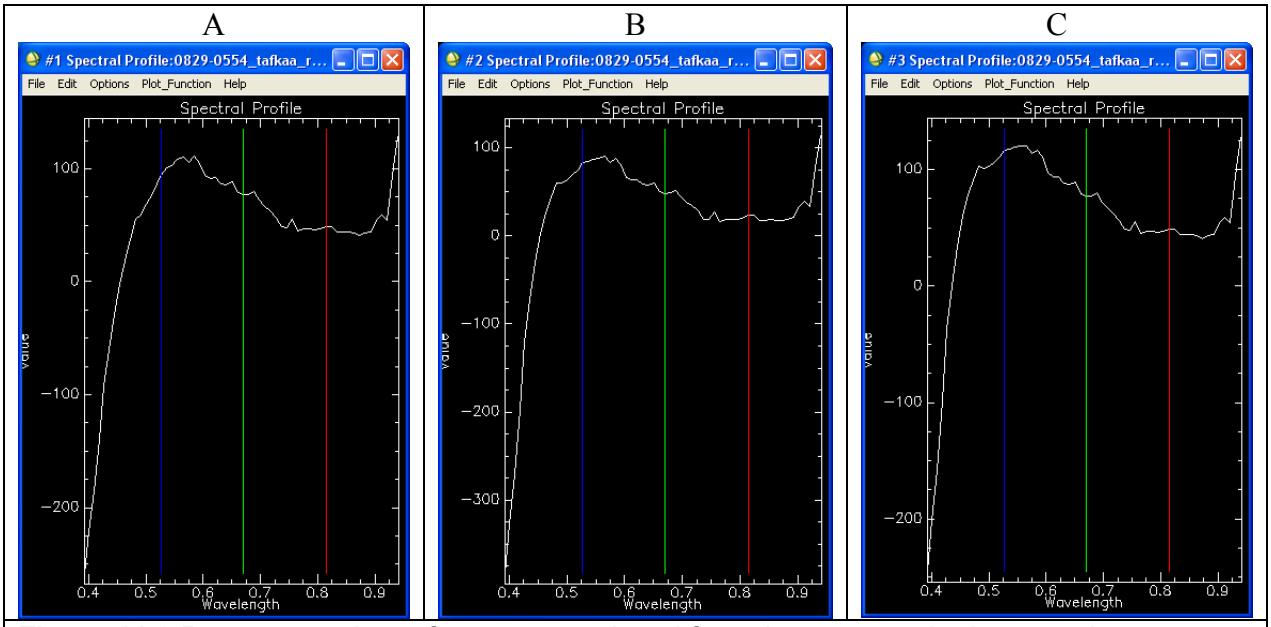

Figure 11.8 Remote sensing reflectances retrieved from three atmospheric correction scenarios. A) No aerosol correction, B) increased NO2 by a factor of 90, and C) a combination of the other two.

11.2.4. Oxygen mapping

Oxygen (O2) is a well mixed gas in the atmosphere. The oxygen absorption is in 765 nm and can be used as a good indicator for several radiometric calibration issues. A shift in location between the MODO-simulated oxygen absorption and the hyperspectral dataset would indicate if there is a problem with the hyperspectral data. Results from the AISA dataset show that the there was a good match between the two absorption locations.

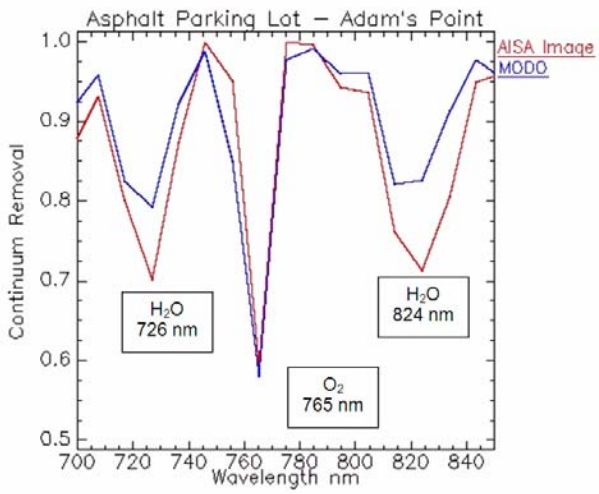

Figure 11.9 Spectral comparison of an oxygenabsorption (Adam's Point) after a continuum removal normalization of the radiance values. The blue and red lines represent the AISA image and the field measurement simulated by MODO, respectively. In addition to the oxygen absorption (765 nm) the water (H_2O) absorption (726 nm and 824 nm) is also noticed.

11.2.5. QA summary

The evaluation of the hyperspectral dataset was conducted by two independent methods: simulated atmospheric model independent from the dataset (MODO) and simulated atmospheric model based on the hyperspectral dataset (TAFKAA). Oxygen mapping test was also conducted on the dataset. Both methods showed AISA spectra above 0.55 microns (550 nm). The AISA imagery reflectance below 0.55 microns diverge significantly from both the comparison methods.

These results were indicative of problems associated with instrumentation and not the atmospheric correction at these blue wavelengths. To verify the approach taken we consulted with Marcos Montes of the Naval Research Laboratory who is the research physicist responsible for the current development of the Tafkaa atmospheric correction software. He agreed that this issue was probably an instrument/calibration/processing problem. This conclusion was shared by Oliver Weatherbee of SpecTIR and appears to be due to problems associated with their calibration source for the instrument and it traceability to NIST. SpecTIR are working to fix this problem but at the time of writing this report no solution was available.

The approach taken in order to continue with the study was to re-process the radiance level dataset and convert it to a reflectance dataset using TAFKAA. The spectral information below 0.55 microns cannot be used. According to data provided, the processing and analysis for the study focused only upon the spectral range above 0.55 microns.

11.3. Available digital elevation model (DEM) of Great Bay Estuary

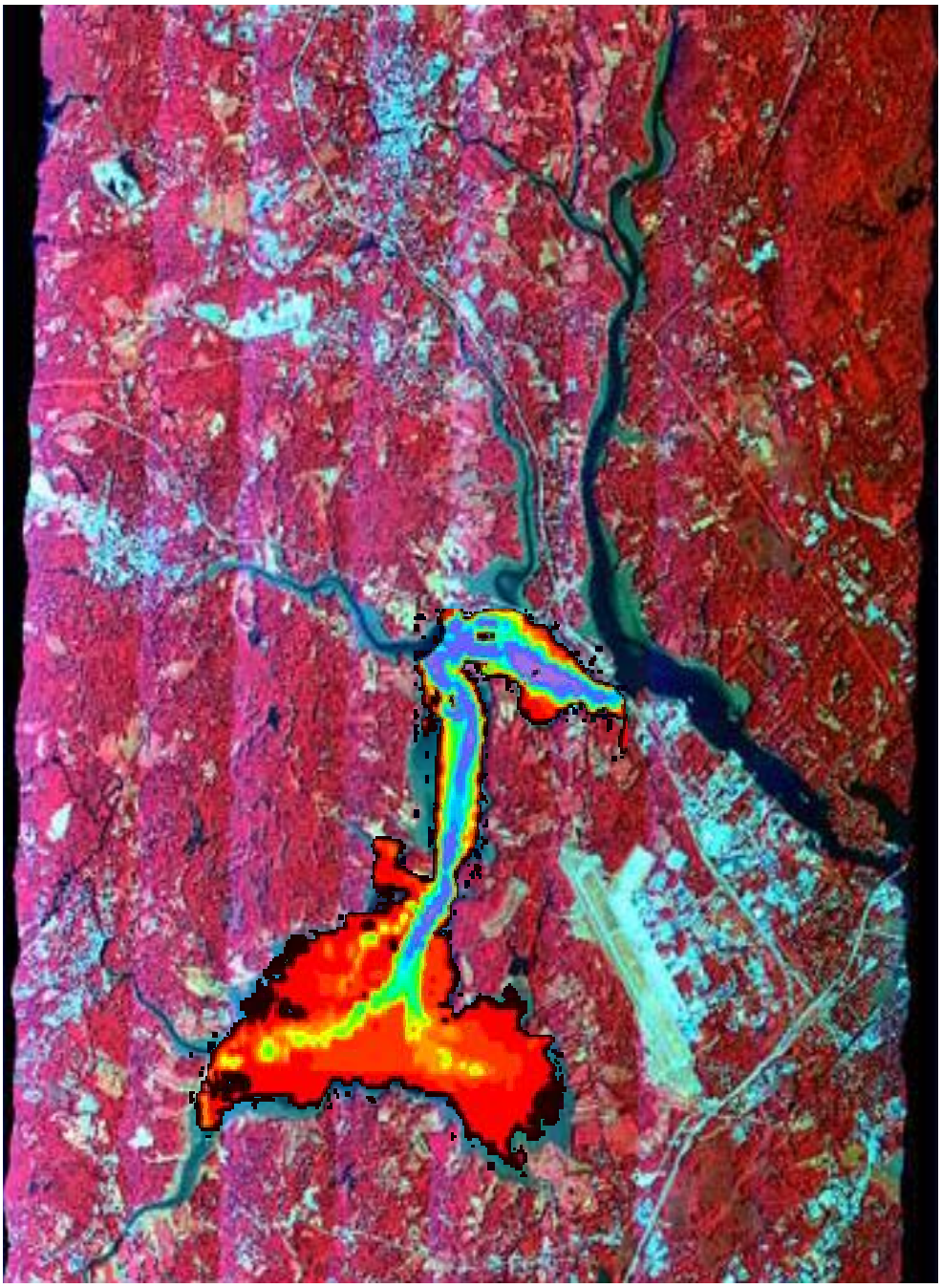

Figure 11.10 NHDES (2008) available DEM

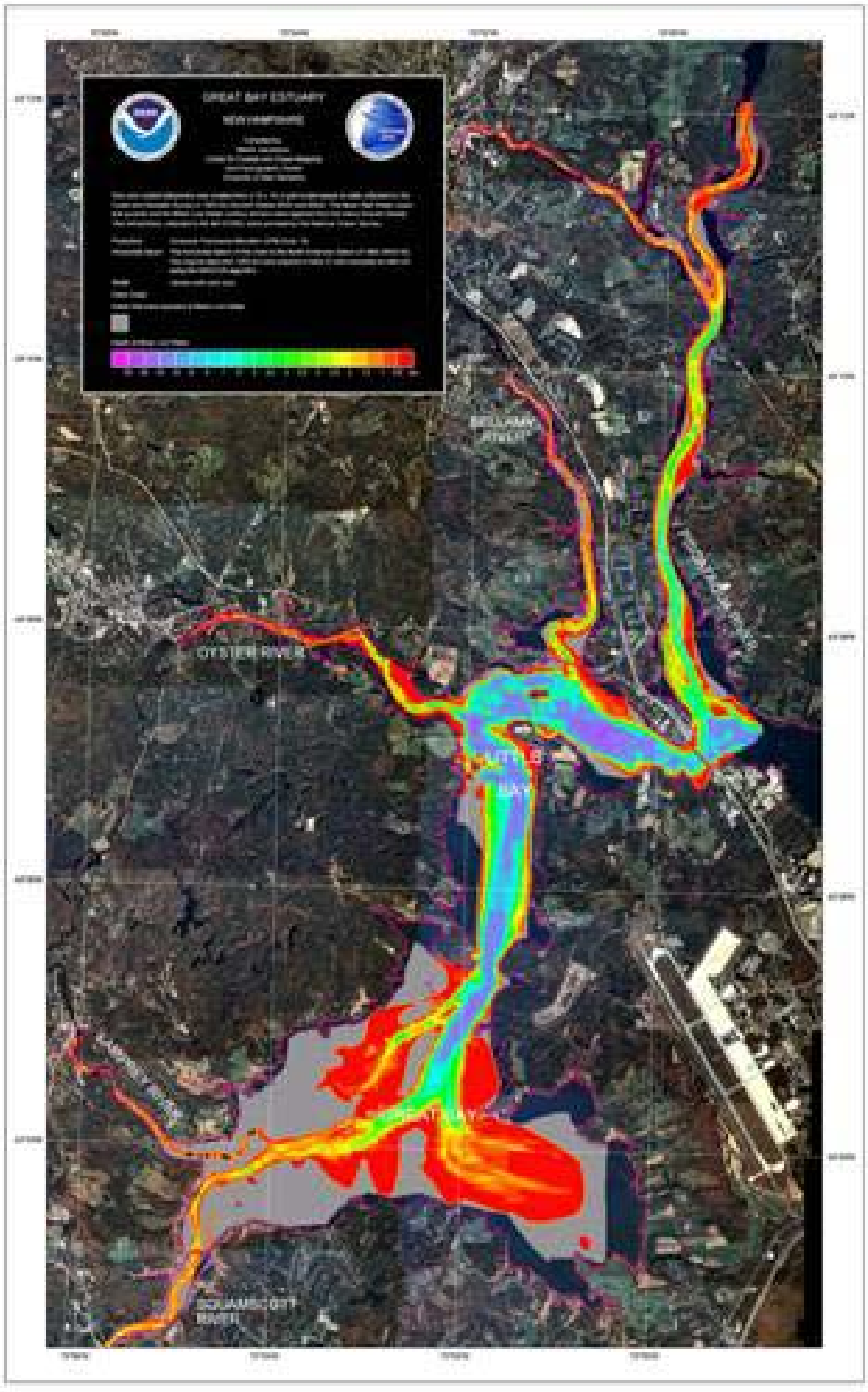

Figure 11.10 USACE (1953) available DEM.

12 References

Alberotanza L R. M. Cavalli, S. P., and A. Zandonella, 2006. Classification of submerged aquatic vegetation of the Venice lagoon using MIVIS airborne data. Annals of Geophysics, **49**(1): 271-276.

Broge, N., and E. Leblanc, 2000. Comparing prediction power and stability of broadband and hyperspectral vegetation indices for estimation of green leaf areas indices and canopy chlorophyll density. Remote Sensing Environment **76:** 156–172.

Dierssen, H. M., R. C. Zimmerman, R. A. Leathers, T. V. Downes, and C. O. Davis, 2003. Ocean color remote sensing of seagrass and bathymetry in the Bahamas Banks by high-resolution airborne imagery. Limnology and Oceanography **48:** 444-455.

Hauxwell et al., 2003. Eelgrass Zostera marina loss in temperate estuaries: relationship to land-derived nitrogen loads and effect of light limitation imposed by algae. Marine Ecology Progress Series, 247: 59-73.

Haxo, F. T. and L. R. Blinks, 1950. Photosynthetic action spectra of marine algae. The Journal of General Physiology **33:** 389-422.

Gao, B., M. J. Montes, Z. Ahmad, and C. O. Davis, 2000. Atmospheric correction algorithm for hyperspectral remote sensing of ocean color from space. Applied Optics **39**: 887-896.

Gitelson, A. (1992): The peak near 700 nm on radiance spectra of algae and water: relationship of its magnitude and position with chlorophyll concentration, International Journal of Remote Sensing **13**: 3367-3373.

Gordon, H. R., O. B. Brown, R. H. Evans, J. W. Brown, R. C. Smith, K. S. Baker, D. K. Clark 1988, A semianalytic radiance model of ocean color. Journal of Geophysical Research **93**: 10909-10924.

Gordon, H. R. 1989. Can the Lambert-Beer law be applied to the diffuse attenuation coefficient of ocean water? Limnology and Oceanography **34**: 1389-1409.

Goodman, J. A., Z-P Lee, and S. L. Ustin 2008, Influence of atmospheric and sea-surface corrections on retrieval of bottom depth and reflectance using a semi-analytical model: a case study in Kaneohe Bay, Hawaii. Applied Optics **47(28)**: F1-F11, doi:10.1364/AO.47.0000F1.

Jacquemoud, S., S. Ustin, J. Verdebout, J. Schmuck, G. Andreoli, AND B. Hosgood 1996, Estimating leaf biochemistry using the PROPSECT leaf optical properties model. Remote Sensing Environment **56**: 194–202.

LaCarpa, V., J. Melack, M. Gastil, and D. Valeriano 1996, Remote sensing of foliar chemistry of inundated rice with imaging spectrometry. Remote Sensing Environment **55**: 50–58.

Lee, Z. P., K. L. Carder, C. D. Mobley, R. G. Steward, and J. S. Patch 1998, Hyperspectral remote sensing for shallow waters. I. A semianalytical model. Applied Optics **37**: 6329-6338.

Lee 1999, Hyperspectral remote sensing for shallow waters: 2. Deriving bottom depths and water properties by optimization. Applied Optics **38**: 3831-3843.

Lee, Z., K. L. Carder, R. F. Chen, and T. G. Peacock 2001, Properties of the water column and bottom derived from Airborne Visible Infrared Imaging Spectrometer (AVIRIS) data. Journal of Geophysical Research-Oceans **106**: 11639-11651.

Lee, Z.-P., and K. L. Carder 2005, Hyperspectral remote sensing, p. 181-204. In R. L. Miller, C. E. Del Castillo and B. A. McKee [eds.], Remote sensing of coastal aquatic environments. Springer.

Lee, K.S., F.T. Short, D.M. Burdick 2004, Development of a nutrient pollution indicator using the seagrass, Zostera marina, along nutrient gradients in three New England estuaries. Aquatic Botany, **78**: 197–216.

Lee, Z. P., K. L. Carder, C. D. Mobley, R. G. Steward, and J. S. Patch. 1998, Hyperspectral remote sensing for shallow waters. I. A semianalytical model. Applied Optics **37**: 6329-6338.

Lee, Z., K. L. Carder, R. F. Chen, and T. G. Peacock. 2001, Properties of the water column and bottom derived from Airborne Visible Infrared Imaging Spectrometer (AVIRIS) data. Journal of Geophysical Research-Oceans **106:** 11639-11651.

Lee, Z.P,. 1999, Hyperspectral remote sensing for shallow waters: 2. Deriving bottom depths and water properties by optimization. Applied Optics **38:** 3831-3843.

Lee, Z.-P., and K. L. Carder. 2005, Hyperspectral remote sensing, p. 181-204. *In* R. L. Miller, C. E. Del Castillo and B. A. MckEE [eds.], Remote sensing of coastal aquatic environments. Springer.

Lesser, M. P., and C. D. Mobley. 2007, Bathymetry, water optical properties, and benthic classification of coral reefs using hyperspectral remote sensing imagery. Coral Reefs **26:** 819-829.

Louchard, E. M., R. P. Reid, F. C. Stephens, C. O. Davis, R. A. Leathers, AND T. V. Downes. 2003, Optical remote sensing of benthic habitats and bathymetry in coastal environments at Lee Stocking Island, Bahamas: A comparative spectral classification approach. Limnology and Oceanography **48**: 511–521.

Lyzenga, D. R. 1981, Remote sensing of bottom reflectance and water attenuation parameters in shallow water using aircraft and Landsat data. International Journal of Remote Sensing **2:** 71-82.

Maritorena, S., A. Morel, and B. Gentili. 1994. Diffuse reflectance of oceanic shallow waters: Influence of water depth and bottom albedo. Limnology and Oceanography **39**: 1689-1703.

Mobley, C. D 1994, Light and water: radiative transfer in natural waters. Academic Press, Inc.

Mobley, C. D., L. K. Sundman, C. O. Davis, J. H. Bowles, T. V. Downes, R. A. Leathers, M. J. Montes, W. P. Bissett, D. D. R. Kohler, R. P. Reid, E. M. Louchard, and A. Gleason 2005, Interpretation of hyperspectral remote-sensing imagery by spectrum matching and look-up tables. Applied Optics **44:** 3576-3592.

Montes, M. J., B. Gao, and C. O. Davis 2001, A new algorithm for atmospheric correction of hyperspectral remote sensing data., p. 23-30. *In* W. E. Roper [ed.], Geo-Spatial Image and Data Exploitation II. SPIE.

Montes, M.J. 2003, Tafkaa atmospheric correction of hyperspectral data, p. 188-197. *In* S. S. Shen and P. E. Lewis [eds.], Imaging Spectrometry IX. SPIE.

NHEP 2006, State of the Estuaries. New Hampshire Estuaries Project, University of New Hampshire, Durham, NH. (url: www.nhep.unh.edu).

Rundquist, D.C., L. Han, J.F. Schalles and J.S. Peake 1996, Remote measurement of algal chlorophyll in surface waters: the case of the first derivative of reflectance near 690 nm, Photogrammetric Engineering and Remote Sensing **63(2)**: 195-200.

Sandage, J. C., and R. J. Holyer. 1998, Coastal bathymetry from hyperspectral observations of water radiance. Remote Sensing Environment **65**: 341-352.

Short, F.T. (ed.). 1992. The Ecology of the Great Bay Estuary, New Hampshire and Maine: An Estuarine Profile and Bibliography. NOAA - Coastal Ocean Program Publ. 222 pp.

Short, F. T., and D. M. Burdick 1996, Quantifying eelgrass habitat loss in relation to housing development and nitrogen loading in Waquoit Bay, Massachusetts. Estuaries **19:** 730-739.

Short, F.T., A.C. Mathieson and J.I. Nelson. 1986. Recurrence of the eelgrass wasting disease at the border of New Hampshire and Maine, USA. Marine Ecology Progress Series **29**:89-92.

SpecTIR 2007, SpecTIR Project Report, NH Department of Environmental Services report, 1148-New Hampshire, 1-11.

Thorhaug, A., A. D. Richardson and G. P. Berlyn 2007, Spectral reflectance of the seagrasses: Thalassia testudinum, Halodulewrightii, Syringodium filiforme and five marine algae, International Journal of Remote Sensing, **28(7)**: 1487–1501.

Philpot, W. D., 1989, Bathymetric mapping with passive multispectral imagery, Applied Optics **28(8)**: 1569-1578

Wezernak, C.T., R.E. Turner and D.R. Lyzenga, 1976: Spectral reflectance and radiance characteristics of water pollutants, NASA CR-2665, 110-111.

Zimmerman, R. C. 2003, A biooptical model of irradiance distribution and photosynthesis in seagrass canopies, Limnology and Oceanography **48**(1, part 2): 568–585.